Thermal Interface Material Characterization Under Thermo-mechanical Stress of Induced Angle of Tilt

by

Enisa Harris

A Thesis Presented in Partial Fulfillment
of the Requirements for the Degree
Master of Science

Approved November 2011 by the
Graduate Supervisory Committee:

Patrick Phelan, Chair
Ronald Calhoun
Shankar Devasenathipathy

ARIZONA STATE UNIVERSITY

December 2011

ABSTRACT

Thermal interface materials (TIMs) are extensively used in thermal management applications especially in the microelectronics industry. With the advancement in microprocessors design and speed, the thermal management is becoming more complex. With these advancements in microelectronics, there have been parallel advancements in thermal interface materials.

Given the vast number of available TIM types, selection of the material for each specific application is crucial. Most of the metrologies currently available on the market are designed to qualify TIMs between two perfectly flat surfaces, mimicking an ideal scenario. However, in realistic applications parallel surfaces may not be the case. In this study, a unique characterization method is proposed to address the need for TIMs characterization between non-parallel surfaces.

Two different metrologies are custom-designed and built to measure the impact of tilt angle on the performance of TIMs. The first metrology, Angular TIM Tester, is based on the ASTM D5470 standard with flexibility to perform characterization of the sample under induced tilt angle of the rods. The second metrology, Bare Die Tilting Metrology, is designed to validate the performance of TIM under induced tilt angle between the bare die and the cooling solution in an “in-situ” package testing format.

Several types of off-the-shelf thermal interface materials were tested and the results are outlined in the study. Data were collected using both metrologies for all selected materials. It was found that small tilt angles, up to 0.6°, have an impact on thermal resistance of all materials especially for in-situ testing. In addition, resistance change between 0° and the selected tilt angle was found to be in close agreement between the two metrologies for paste-based materials and phase-change material. However, a clear difference in the thermal performance of the tested materials was observed between the two metrologies for the gap filler materials.

DEDICATION

This research is dedicated to my children Din and Mak whose bright smiles bring joy to my life. It is my greatest hope they understand it's never too late to pursue your dreams.

ACKNOWLEDGMENTS

I would like to thank my advisor, Dr. Patrick Phelan for his invaluable guidance and also Dr. Shankar Devasenathipathy, my mentor, without their help this research would not have been completed. I would also like to thank Dr. Ronald Calhoun for dedicating his time to my thesis defense. In addition, I would also like to thank all of my peers who I work with in the lab. I am indebted to my husband, James Harris, and my mother, Enisa Rustempasic, for their altruism, support, and encouragement. Funding for this research was provided by Intel Corporation.

TABLE OF CONTENTS

Page

CHAPTER Page

LIST OF TABLES

LIST OF FIGURES

Figure Page

Figure Page

Figure Page

Figure Page

LIST OF SYMBOLS

A, area

BLT, bond line thickness

IHS, integrated heat spreader

L, thickness

P, power

PCM, phase change material

R, thermal resistance

R_{area}, thermal impedance

R_{con}, conduction thermal resistance across TIM

$R_{contact1}$, contact thermal resistance with surface 1

$R_{contact2}$, contact thermal resistance with surface 2

$R_{int,}$ interface thermal contact resistance

T_{CPU}, electronic package temperature

T_{hs}, heat sink temperature

TDP, total design power

TIM, thermal interface material

T_j, junction temperature (temperature of bare die)

T_p, temperature of the cold block (temperature of the plate)

ΔT, temperature difference

k, thermal conductivity

k_{air}, air thermal conductivity

k_{eff}, effective thermal conductivity of TIM

$k_{TIM,}$ bulk thermal conductivity of TIM

q, heat flux

$\frac{\partial R_{cond}}{\partial L}$, derivative of conduction contact resistance with respect to TIM thickness

$\frac{\partial R_{contact}}{\partial L}$, derivative of contact resistance with respect to TIM thickness

$\frac{\partial R_{int}}{\partial L}$, derivative of interface resistance with respect to TIM thickness

θ_{jp}, thermal resistance junction to plate

$\theta_{jp@angle}$, thermal resistance at specific tilt angle

$\theta_{jp@0}$, thermal resistance at 0° tilt angle

$\Delta\theta_{jp}$, thermal resistance difference between thermal resistance at specific tilt angle and thermal resistance at 0° tilt angle

Chapter 1

INTRODUCTION

Since the 1960's, the microelectronic industry has followed Moore's Law [1], stating that the number of transistors on a chip roughly doubles every two years. As a result the design scale of the microprocessors is getting smaller and the power density and heat dissipation increases. The importance of thermal management within the overall product design continues to increase and is becoming one of the most important aspects of the overall design. Selection of the thermal interface material (TIM) is becoming an integral part of the overall thermal design process.

The reliability and life of the semiconductor component is highly dependent on its operating conditions especially its operating temperature. For this reason, the heat generated within the component must be removed to insure a safe operating limit for the component's junction temperature. Junction temperature is the temperature of the actual semiconductor in an electronic device. Computer manufacturers specify maximum junction temperatures from 65°C to 105°C depending on the desired reliability levels [2].

1.1 Thermal Interface Materials

As selection of the TIM plays a key role in thermal management design, various TIMs have been developed. Recent studies have shown enhancements in thermal interface materials with carbon nanotube arrays

[3, 4]. Nano-TIMs, manufactured by eletrospinning process, with nano-SiC particles distributed in the matrix to enhance the thermal conductivity and decrease the thermal resistivity were also developed [5]. Other high conductivity materials, such as graphite, also play a key role in new TIM development [6].

With the vast number of new as well as traditional TIMs, having a basic understanding of their strengths, weaknesses, and applicability is a key to successful selection of the best interface material. The selection of proper TIM depends on many factors like power density, heat dissipation, process requirements, Bond Line thickness (BLT), rework ability and user preferences [7]. Based on these basic properties TIMs can be categorized into the families summarized in Table 1 [8].

Table 1. Family of commercially available TIMs.

TIM Category	Thickness (in)	Available Reinforcing Carriers	Dielectric Strength (Vac)	Thermal Impedance (C-cm^2/W)	Thermal Conductivity (W/mK)	Typical Cost ($/sq in)
Elastomeric Pads/Insulators	0.003 to 0.03	Fiberglass Aluminum Foil Kapton	2000 to 14000	0.15 to 0.65	0.7 to 3.0	0.03 to 0.3 0.06 typ.
Thermally Conductive Adhesive Tapes	0.005 to 0.015	Free Film Fiberglass Aluminum Foil Expanded Aluminum Kapton	0 to 6.0	0.20 to 1.5	0.3 to 1.7	0.06 to 0.3 0.15 typ
Phase-Change Materials	0.002 to 0.012 preform 0.001 to 0.008 final bond line thickness	Free Film Fiberglass Aluminum Foil Aluminum Kapton	2.00 to 5.00 (for dielectric carrier versions only)	0.02 to 0.25 0.4 to 0.5 dielectric version	0.5 to 1.9	0.06 to 0.30 0.12 typ
Thermally Conductive Gap Fillers	0.02 to 0.30	Molded Parts Internal Fiberglass External Fiberglass Aluminum Foil Polyester	100 to 400 V/mil	0.3 to 4.0	0.7 to 5.0	0.20 to 0.90 0.30 typ
Thermally Conductive Cure-in-Place Compounds			100 to 400 V/mil	0.3 to 4.0	0.7 to 3.0	0.12 to 0.45 0.35 typ
Thermal Compounds or Greases	0.0005 to 0.005 final bond line thickness			0.02 to 0.20	0.7 to 4.0	0.01 to 0.12 0.02 typ
Thermally Conductive Adhesives	0.003 to 0.025			0.08 to 0.40	0.7 to 4.0	0.03 to 0.20 0.08 typ

1.1.1 Elastomeric Pads/Insulators

Elastomeric pads/insulators were developed for application between discrete power devices and heat sinks. This class of product is

characterized by high thermal conductivity, very high dielectric strength, and volume resistivity. To work effectively, thermal pads require very high (greater than 1400kPa (200 psi)) clamping pressures [8].

1.1.2 Thermally Conductive Adhesive Tapes

Thermally conductive adhesive tapes are acrylic or silicone pressure-sensitive adhesive tapes used extensively to bond heat sinks to microprocessors and other heat-generating microelectronic components. Critical practical performance factors for tapes include peel strength, lap- and die-shear strength, holding power, and thermal resistance [9]. These tapes have moderate thermal conductivity, and their thermal performance highly depends on the contact area between the bonding surfaces. For the most part, the quality of the two joining surfaces would determine the amount of contact achieved and the expected thermal performance. Shear strength decreases as tape thickness increases, and is also dependent on the substrate type for this TIM type.

1.1.3 Phase Change Materials (PCMs)

Phase-change materials have a comparable thermal performance with thermal grease type materials but ease of handling and installation that of pad-type TIMs. They are capable of operating in two states - solid and liquid - over their specified temperature range. Phase-change materials are solid at room temperature and behave like paste above their melting temperature. The temperature at which the transition from solid to

liquid state occurs is defined as the melting point or phase-change temperature. The melting point for typical products available ranges from 50-90°C [10]. These materials do not provide electrical isolation because they may allow the two surfaces to come in contact.

1.1.4 Thermally Conductive Gap Fillers

Thermally conductive gap fillers are low-modulus, thermally conductive silicone elastomers for applications where heat must be conducted over large gaps between hot components and a cold surface. Therefore, gap fillers are sufficiently pliant to fill such gaps. These materials have moderate thermal conductivity [11].

1.1.5 Thermally Conductive Cure-In-Place Compounds

Thermally conductive cure-in-place compounds have properties similar to the thermally conductive gap fillers described above once they are cured. They are reactive, one- or two-part silicone room-temperature vulcanizing or similar compounds that can be used to form thermal pathways in applications where the distance between a component and a cold surface is highly variable. A typical application would be a PC board with many different height components that need to be brought into contact with a chassis or heat sink [8].

1.1.6 Thermal Compounds or Greases

Thermal compounds or greases are by far the most commonly used TIMs. Thermal greases are most commonly conducting particle-(usually metal or metal oxide) filled silicone [12-15]. The bulk thermal conductivity of thermal greases is not high. However, because the paste-like consistency of these materials allows very thin bond line thickness (BLT), the thermal impedance across this TIM can be quite low.

The downside of the thermal greases is that it can separate and dry out over time. Repeated power on/off cycles during operation of the microprocessor, can result in thermal grease pump-out, which causes significant degradation in thermal performance over time [16, 17]. Figure 1 shows the effect of grease pump-out on thermal performance post power cycles.

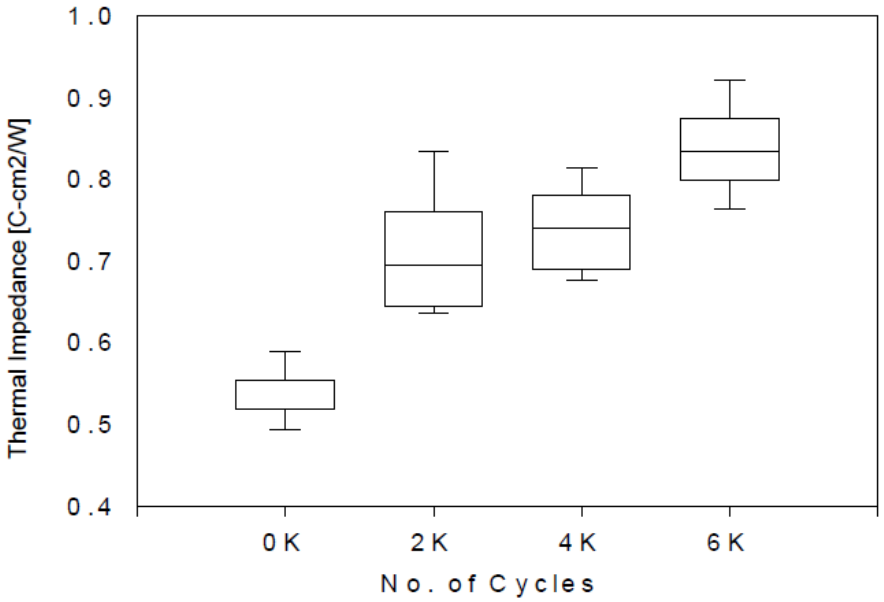

Figure 1.Thermal grease thermal impedance measurement post power cycles [12].

Figure 2 and Figure 3 show observed grease pump-out after 4000 and 6000 power cycles respectively.

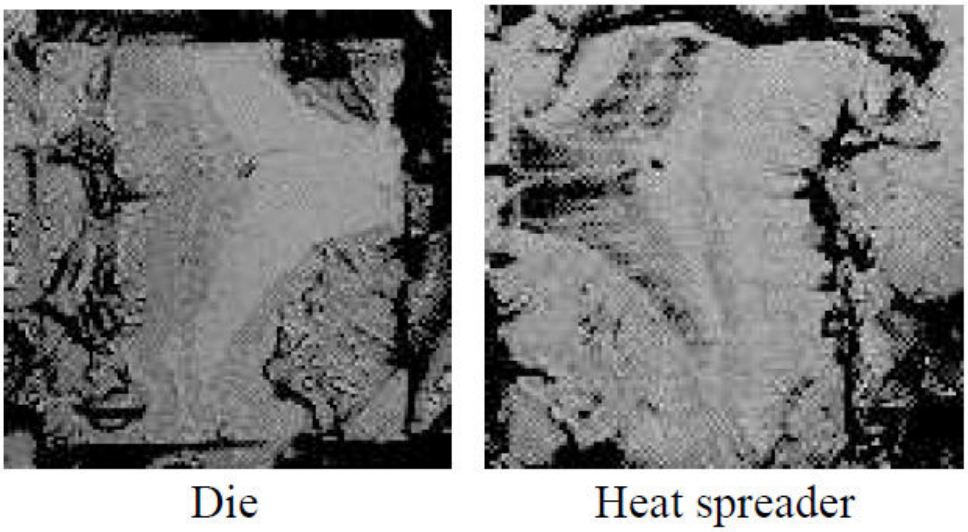

Figure 2. Observed grease pump-out post 4000 power cycles [16].

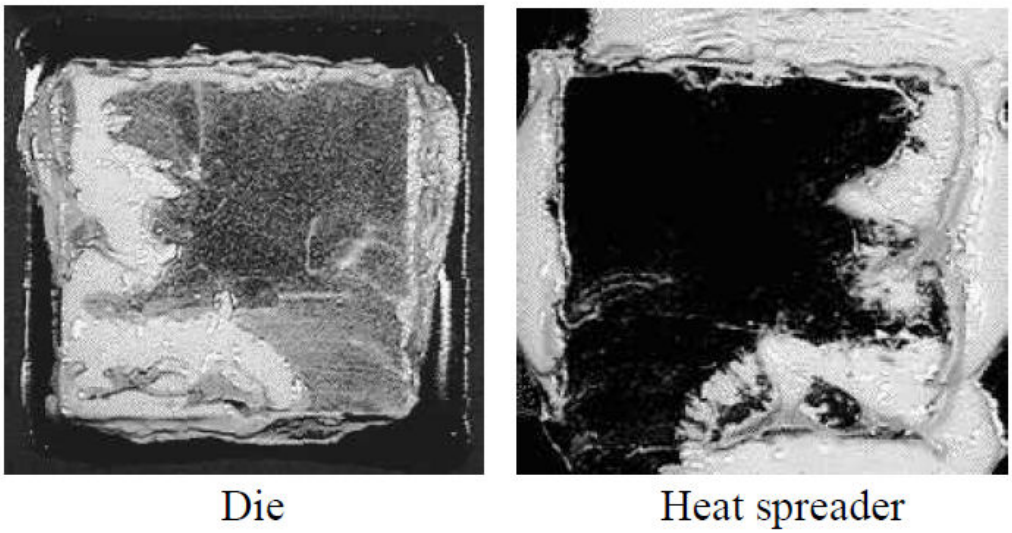

Figure 3. Observed grease pump-out post 6000 power cycles [16].

1.1.7 Thermal Adhesives

Thermal adhesives are one- or two-part adhesive compounds. To enhance the bulk thermal conductivity, ceramic fillers are typically added to the compound. They are typically used to bond small heat sinks to low power electronic components.

1.2 Motivation

Integrated heat spreader (IHS) or heat sink assembly to microprocessor can be complex. Generally, the tilt of the cooling solution is not controlled as the heat sinks are attached using torque screwdrivers. The assembly of the IHS is even more complex as it generally done by applying the epoxy between the heat spreader and the component substrate. An ideal IHS attach process requires optimizing the adhesive material, adhesive dispense pattern, adhesive quantity, placement forces, and hold time to achieve both the required bondline thickness of TIM in the chip area and the substrate coupling required to improve module flatness after adhesive cure [18].

An inadequately controlled assembly process may result in a small tilt between the heat sink or the IHS and the microelectronic processor. It is the role of the TIM to fill in the gaps and provide adequate thermal path from the processor to the heat sink and this study explores the ability of selected TIMs to do so.

1.3 Objectives

The objectives of the study are:

1. Development of metrology for fundamental TIM characterization under induced tilt angle
2. In-situ (electronic package scenario) TIM characterization under induced tilt angle
3. Validate proposed metrologies using off-the-shelf TIMs.

To meet the objectives, two types of thermal grease and gap-fillers each at three different perform thicknesses, along with phase-change material, were selected for characterization. The goal is to characterize the capability of these materials to conform to an induced tilt angle.

Chapter 2

BACKGROUND

Over the past decades, the evolution of microprocessors has led to an increase in cooling demand due to an increase in raw power (or total design power TDP) as well as local power densities known as “hot spots” [19-22]. A historical trend chart for Intel-based microprocessor TDP vs. frequency is shown in Figure 4 while Figure 5 illustrates a typical die power map and corresponding temperature hot spot.

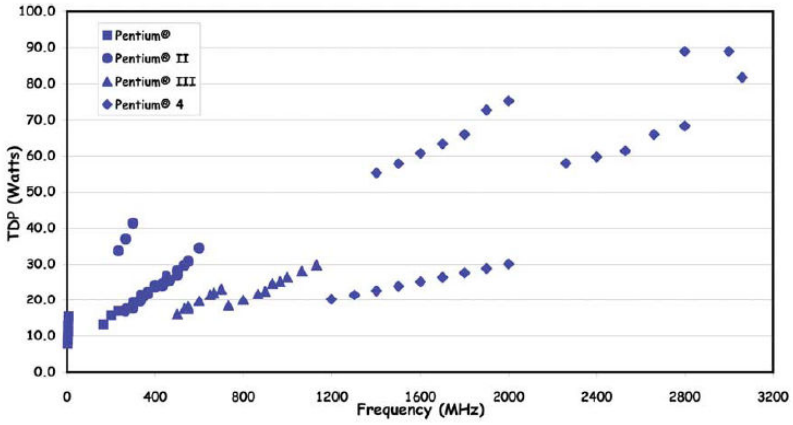

Figure 4. Historical trend chart of microprocessor TDP versus frequency [22].

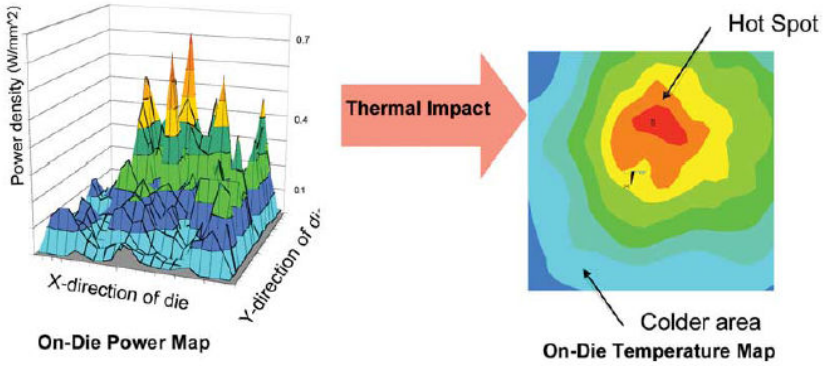

Figure 5. Schematic illustrating typical die power map and the hot spots on the corresponding die temperature map. The red region represents the highest temperature spot [22].

With the increasing power density in microelectronics industry, thermal design and selection of thermal interface materials has become critical. It is essential for the generated heat to be removed from the electronic package to meet the performance and reliability of the component. The heat removal process is generally done by means of a heat sink attached to the semiconductor component. The primary heat path for both bare die and lidded semiconductor packages is depicted in Figure 6.

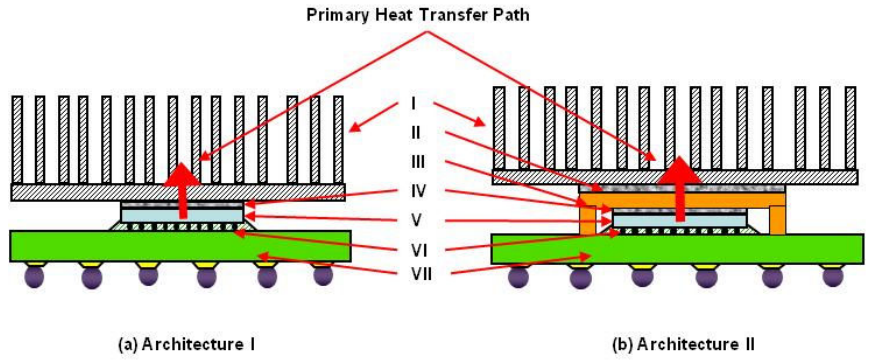

Figure 6. Schematic illustration of the two thermal architectures: (a) Architecture I is typically used in laptop applications. (b) Architecture II is typically used in desktop and server (Legend: I – Heat Sink, II – TIM, III – IHS, IV – TIM, V – Die, VI – Underfill, and VII – Package Substrate).

Architecture I, depicted in Figure 6 and generally used in laptop applications, is a bare die scenario. In this case, the TIM is applied directly to the silicone and the heat sink is attached on top. For architecture II, generally used in desktop or server configurations, a heat spreader is used along with the heat sink. In such applications, there are two separate TIMs applied which are generally of different types. The

first, TIM1, is used between the silicon die and the heat spreader and the second, TIM2, is used between the heat spreader and the heat sink. In both architectures, the TIM plays a key role in heat removal from the semiconductor device [19].

The role of the TIM is to bring two surfaces, heat generating and heat removing surfaces, into intimate thermal contact and therefore reduce thermal resistance between the surfaces. Commercial grade surfaces, such as those of the heat sink, heat spreader or semiconductor device, have microscopic surface roughness and generally macroscopic non-planarity. These characteristics can give the surfaces a concave, convex or twisted shape as illustrated in Figure 7.

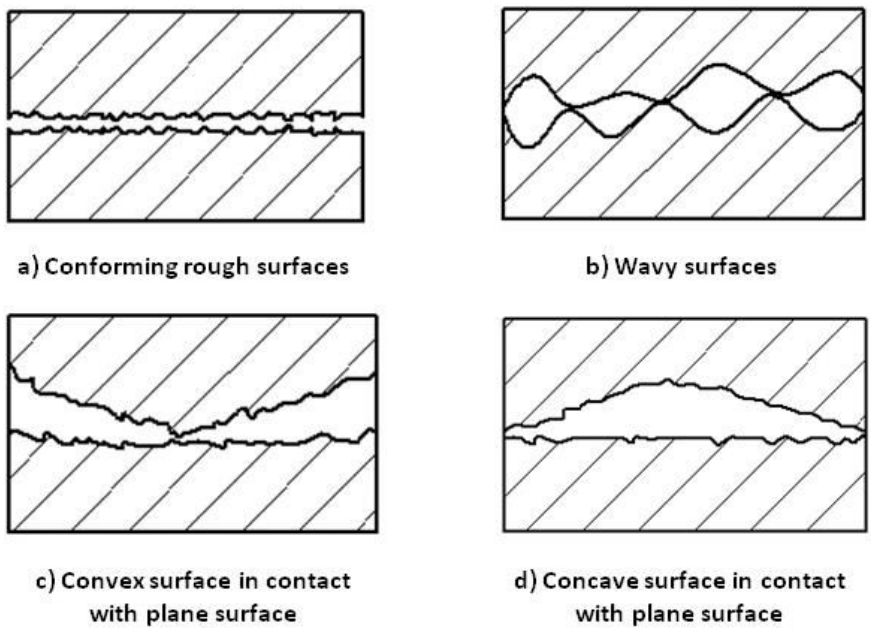

Figure 7. Surface contact configurations.

As apparent from Figure 7, when such surfaces come in contact, the actual contact only occurs at high points and the remainder forms air-filled gaps. Typical contact area can consist of more than 80% air voids [8]. As air has a very low thermal conductivity (k_{air} = 0.026 W/mK at room temperature), these air-filled gaps have high thermal resistance i.e. high resistance to heat flow. With high thermal resistance, the component junction temperature increases.

Therefore, the goal of the TIM is to minimize these gaps by conforming to the uneven surfaces and reduce the overall thermal resistance of the contact. TIMs have higher thermal conductivity than air and hence when properly selected and utilized, reduce the thermal resistance and ultimately the component junction temperature.

The thermal performance of a material is generally characterized in terms of its thermal conductivity. For 1-dimensional heat flow in a homogeneous material, Fourier's law is written as [23, 24]

$$q = kA\frac{\Delta T}{L} \tag{1}$$

where k is material thermal conductivity, L the material thickness, ΔT the temperature difference across the material and A the cross-sectional area. From equation (1) the thermal resistance can then be defined as:

$$R = \frac{\Delta T}{q} = \frac{L}{kA} \tag{2}$$

For thermal interface materials, the resistance is a measure of how well heat is transferred across the interface of two surfaces in contact. In

the case of a semiconductor package (CPU) and heat sink interface, the interface resistance (per unit area) can then be written as

$$R_{int} = \frac{T_{CPU} - T_{hs}}{q} \quad (3)$$

where T_{CPU} is the junction temperature of the semiconductor device and T_{hs} the temperature of the heat sink.

Figure 8 illustrates the thermal interface between two surfaces when no TIM and when an ideal TIM is applied.

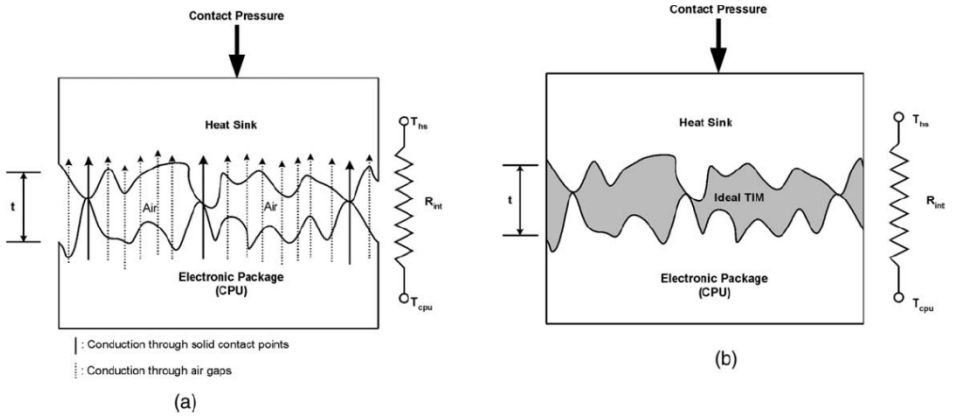

Figure 8. Exploded view of thermal interface when (a) no TIM is used (b) when an ideal TIM is used [25].

The interface when no TIM is applied between two surfaces in contact is the worst case scenario where interface resistance is highest, as the contact between two surfaces occurs only at high points and the rest is air-filled gap. The ideal TIM would be the best-case scenario where the thermal interface resistance would be at a minimum. However, the ideal TIM has not been discovered, and the actual commercially available TIMs would not be able to fill all air gaps. Therefore, Figure 9 illustrates a more realistic interface with a TIM applied.

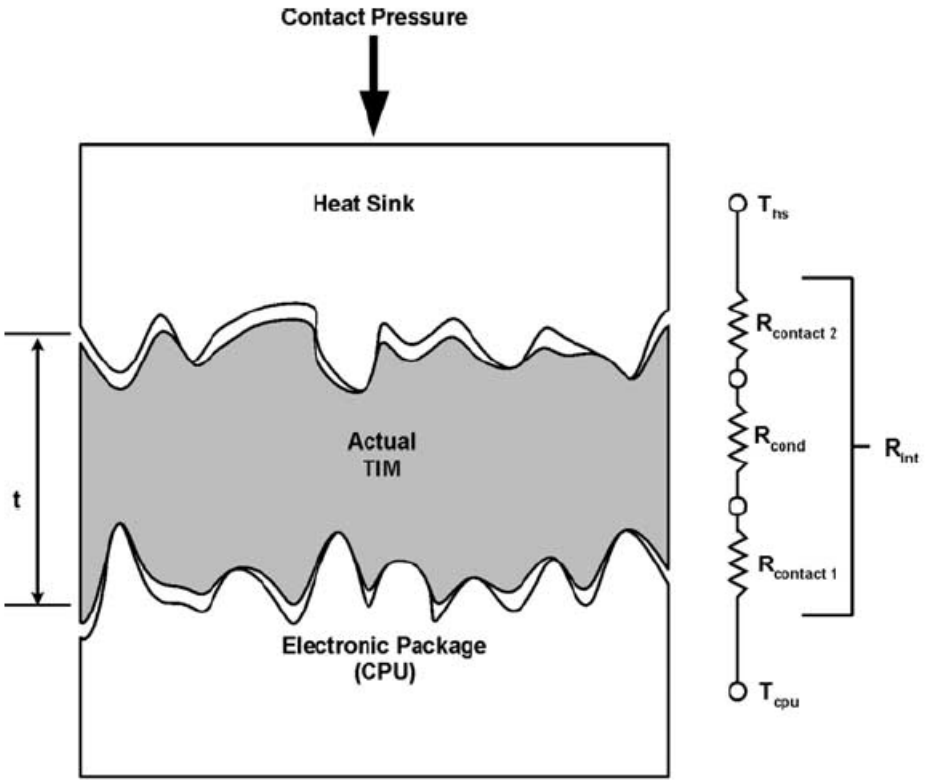

Figure 9. Thermal interface with actual TIM [25].

In the more realistic scenario, the thermal interface resistance is composed of three resistances in series. The total interface resistance can then be expressed as [25]

$$R_{int} = R_{contact1} + R_{cond} + R_{contact2} \quad (4)$$

where R_{int} can also be evaluated from equation (3), $R_{contact1}$ is the contact resistance between the TIM and the CPU surfaces, R_{cond} is the conduction resistance across the TIM, and $R_{contact2}$ is the contact resistance between the TIM and the heat sink.

Combining the contact resistances in equation (4) into a single term, the total contact resistance can then be expressed as:

$$R_{contact} = R_{contact1} + R_{contact2} \quad (5)$$

Therefore, equation (4) can be rewritten as

$$R_{int} = R_{contact} + R_{cond} \quad (6)$$

Taking the derivative of the interface resistance with respect to the material thickness, the above equation can be written [23]:

$$\frac{\partial R_{int}}{\partial L} = \frac{\partial R_{contact}}{\partial L} + \frac{\partial R_{cond}}{\partial L} \quad (7)$$

If it is assumed that the contact resistance is independent of the material thickness, equation (7) can then be reduced to

$$\frac{\partial R_{int}}{\partial L} = \frac{\partial R_{cond}}{\partial L} \quad (8)$$

Using the definition of thermal resistance from equation (2), the thermal resistance of the TIM alone can be expressed as:

$$R_{cond} = \frac{L}{k_{TIM}A} \quad (9)$$

where k_{TIM} is the bulk thermal conductivity of the TIM, L the material thickness and A the cross sectional area. The interface resistance vs. thickness data therefore exhibits a linear relationship as equation (6) can be rewritten as:

$$R_{int} = R_{contact} + \frac{L}{k_{TIM}A} \quad (10)$$

Since $R_{contact}$ is assumed to be constant and the $1/k_{TIM}A$ term is independent of TIM thickness L, equation (10) is simply a straight line with the slope of $1/k_{TIM}A$ and an intercept of $R_{contact}$.

The derivative of the TIM resistance and hence the total interface resistance can then be written as:

$$\frac{\partial R_{cond}}{\partial L} = \frac{1}{k_{TIM} A} = \frac{\partial R_{int}}{\partial L} \tag{11a}$$

The bulk thermal conductivity can be found using:

$$k_{TIM} = \frac{1}{A} \frac{1}{\left(\frac{\partial R_{int}}{\partial L}\right)} = \frac{1}{A} \frac{1}{\left(\frac{\partial R_{cond}}{\partial L}\right)} \tag{11b}$$

Equation (11b) shows that the bulk thermal conductivity of the TIM can be evaluated by determining the slope of the total thermal resistance of the TIM (including contact resistance) with respect to the TIM thickness [26] or

$$k_{TIM} = \frac{1}{Slope} \tag{12}$$

It should be noted that the bulk thermal conductivity is independent of the interfacial contact resistance. Therefore, to obtain the total thermal performance of the TIM interface, the interfacial contact resistance must be accounted for as illustrated in equation (10).

An effective thermal conductivity k_{eff} can also be defined for TIMs. The effective thermal conductivity k_{eff} is defined as [23]:

$$R_{int} = \frac{\Delta T}{q} = \frac{L}{k_{eff} A} \tag{13a}$$

The effective thermal conductivity can then be calculated by:

$$k_{eff} = \left(\frac{L}{A}\right)\left(\frac{q}{\Delta T}\right) = \left(\frac{L}{A}\right)\left(\frac{1}{R_{int}}\right) \tag{13b}$$

It should be noted that equation (13a) incorporates the interfacial contact resistance, as can be seen by comparing equation (13a) with equation (10). Effective thermal conductivity k_{eff} also depends on the thickness of

the TIM, unlike the bulk thermal conductivity k_{TIM} [23, 27, 28]. Another useful parameter is thermal impedance which can be defined as thermal resistance times cross sectional area or

$$R_{area} = RA \tag{14}$$

It is important to notice that the interface resistance is application specific, because of its dependence on mating surface properties. The magnitude of the thermal contact resistance can have a major role in heat management of electronic devices and, hence, may significantly affect performance, reliability and life cycle of such devices [29].

Numerous test methods exist for quantifying thermal conduction characteristics of TIMs. Many tests are carried out using ASTM Test Methods E1530, D5470 and F433 [30, 31]. These methods are generally steady-state 1D heat transfer based. In addition to these, there are transient-based methods and metrologies such as the Laser Flash method [32].

The surface roughness and flatness of the mating surfaces will differ in each application. As R_{int} is application specific, the R_{int} data measured in a given standard test facility mentioned above will not necessarily be applicable to different installations of a TIM.

Thus, the TIM resistance values reported by TIM manufacturers may not be applicable to an actual use case. Further, it is not clear that the use of a heat sink clip will provide uniform pressure on the interface material or that the heat sink will not be slightly tilted, and estimation of

interface resistance based only on the conductivity of the TIM will likely result in an under prediction of R_{int}.

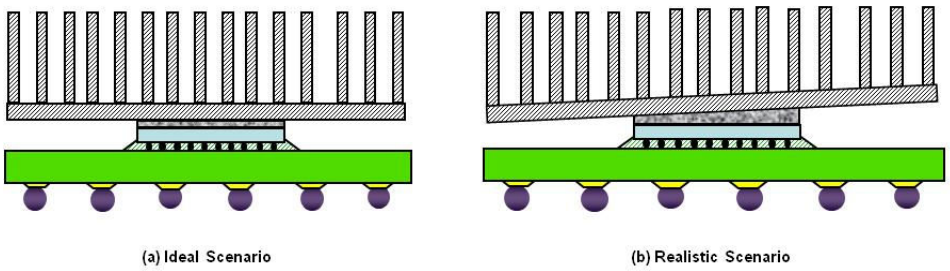

Figure 10. Ideal vs. realistic TIM application scenario.

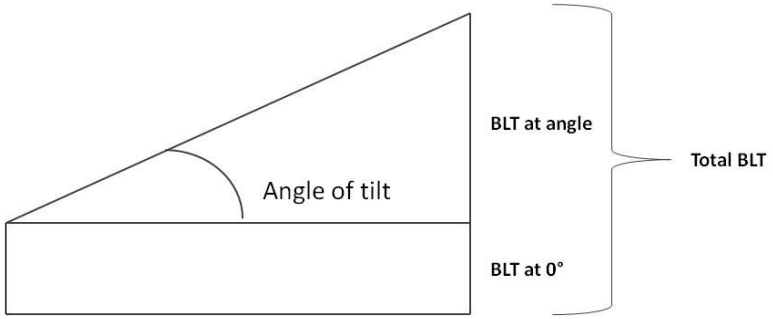

Figure 11. Impact of tilt to TIM bond line thickness (BLT).

Figure 10 depicts the ideal versus more realistic application of the TIM on a bare die package where in a realistic scenario the heat sink may be slightly tilted. To understand the impact of the tilt we can refer to schematic in Figure 11. As discussed previously (equation (13a)) the interface resistance R_{int} is a function of TIM thickness. The thickness of the TIM where tilt is present will be different compared to no tilt scenario. This by itself will impact the R_{int}.

For these reasons, two different metrologies were developed for this study to characterize TIMs. The first metrology estimates interface resistance based on the conductivity of the TIM alone, while the second is an application specific, in-situ method for TIM characterization under induced angle of tilt. Details on both metrologies are discussed in Chapter 3.

Chapter 3

METROLOGY

In this section, design and validation of an Angular TIM Tester for fundamental TIM characterization are detailed. In addition, design and validation of a Bare Die Tilting Metrology are also presented.

3.1 Angular TIM Tester Overview

The Angular TIM Tester developed for this study is based on the ASTM D5470 standard [31] including some improvements specific for TIM characterization between two non-parallel surfaces. The overall dimensions of the tabletop metrology are 14x10x24 inches. Metrology is aligned using high precision bearings, x-y and tilt stages allowing for precise alignment and actuation of the test section. In addition, the tilt stage is used to perform TIM testing under a specific tilt angle. An actuator with LVDT, located at the top of the metrology, is used to drive the test stage while the load cell is utilized for load/stress measurements and control. The schematic of the metrology is illustrated in Figure 12.

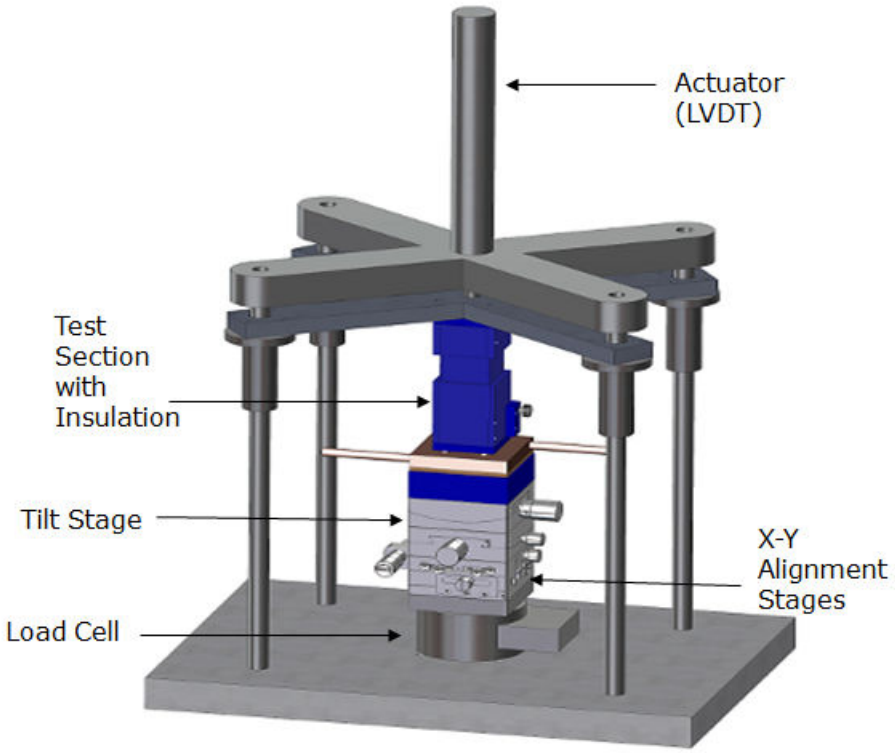

Figure 12. Angular TIM Tester schematic.

The basic idea behind the metrology is to induce one-dimensional heat transfer through the test sample under a known load. To achieve this, two copper rods are utilized. The diameter of each rod is 12.7 mm (0.5 inches) and the length is 38 mm (1.5 inches). Figure 13 illustrates the rods, i.e. the test section.

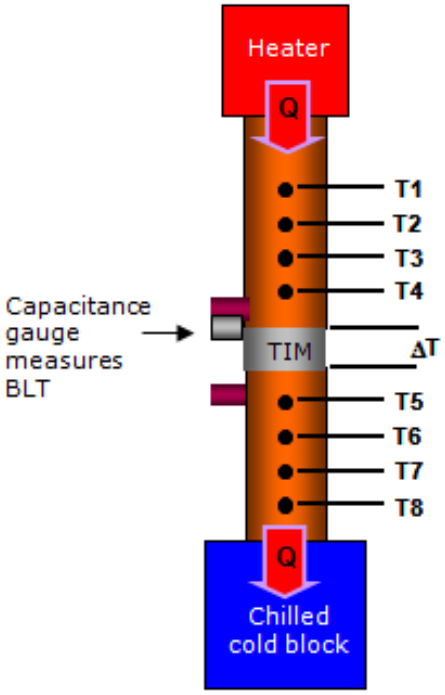

Figure 13. Test section.

The top rod--the heating stage--has two embedded cartridge heaters at the very top used to induce heat flux through the sample. The bottom rod--the cooling stage--has an integrated cold block at the bottom whose temperature is controlled by an external chiller. For precise temperature and heat flux measurements, four k-type 36 gauge thermocouples are embedded along the length of each rod as illustrated in Figure 13. For accuracy of heat flux calculations, the position of each thermocouple was measured in a dimensional laboratory. The thermocouples are positioned approximately 10 mm apart.

A capacitance gauge, Capacitec HPB-75B-V-L3-T-5-BNC, positioned very close to the sample, approximately 1um, is utilized for precise bond line thickness (BLT) measurement of the sample under test.

Positioning the cap gauge close to the sample is critical to accounting for thermal expansion of the rods. This will be discussed in detail in the metrology calibration Section 3.1.2.

The metrology is designed so that tests can be performed under either load (stress) or cap gauge (displacement) control. In either case, measurements are continuously collected as load and thickness are needed to quantify results. As the goal of the project is to characterize TIM performance between two non-parallel surfaces, the metrology is designed so that the center of tilt is located at the top of the cooling stage i.e., the top of the cooling rod. The tilt stage is used to induce the desired tilt of the bottom rod while digital protractor and TekScan™ are utilized to verify the angle.

TekScan™ is high-resolution, thin-film tactile pressure/force sensor array. It is an extremely thin (~0.1 mm) and flexible grid-based device which allows for minimally intrusive measurements, resulting in the least disturbance to the true pressure pattern. The TekScan™ sensor consists of a matrix of rows and columns of a semiconductive material that changes its electrical resistance when force is applied to it. These rows and columns intersect to form sensing elements. By electronically scanning and measuring the change in resistance at each individual sensing element, the timing, force, and location of contacts on the sensor surface can be determined.

3.1.2 Metrology Calibration

The two main metrology parts responsible for the accuracy of the results are the actuator and the capacitance gauge. To insure accurate BLT measurement of the TIM, the cap gauge, located very close to the TIM (i.e test sample), was calibrated. The actuator calibration was performed using a standard calibration method by utilizing high precision gauge blocks. The cap gauge was then calibrated at room and high temperature using the actuator and thermal grease as a medium.

The room temperature calibration was performed under displacement control at 10-um increments and both actuator and cap gauge data were recorded. Both actuator and cap gauge data showed highly repeatable and accurate BLT values as illustrated in Figure 14.

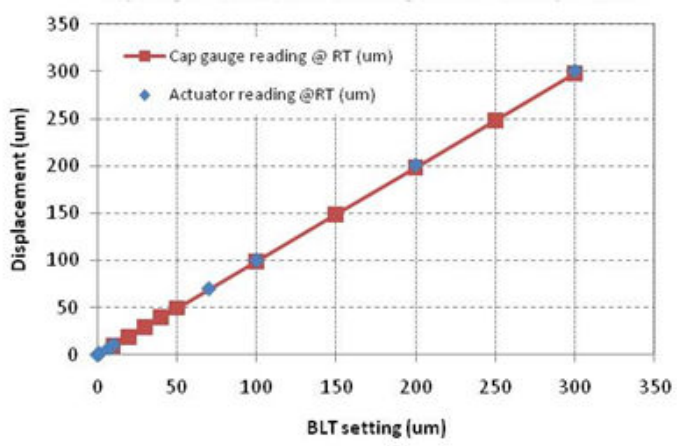

Figure 14. Cap gage and actuator calibration plot at room temperature**.**

For high temperature calibration, to insure one-dimensional heat flow thermal grease was used as a medium between the two rods. The initial BLT of the grease was set to 270 um and data were recorded for

both the actuator and cap gauge. All the measurements were performed under cap gauge displacement control. The BLT was reduced by 50-um increments until the 120-um set-point was reached. After this point, the measurements were taken at 10-um increments. Findings showed very repeatable cap gauge measurements. Small deviation from the set-point of approximately 2 um was observed which was below the target for this project (set to +/- 5 um).

At high temperature 110°C, rods show significant thermal expansion and the actuator is unable to estimate the BLT accurately. However, since the cap gauge is positioned very close to the sample (1 μm), it is able to capture the thermal expansion of the rod and provide a much more accurate BLT measurement and therefore is utilized during calculations of the results. The deviation of the actuator from the set point due to the thermal expansion of the rods and the accuracy of the cap gauge at high temperature are illustrated in Figure 15. Room temperature measurements were used as a reference.

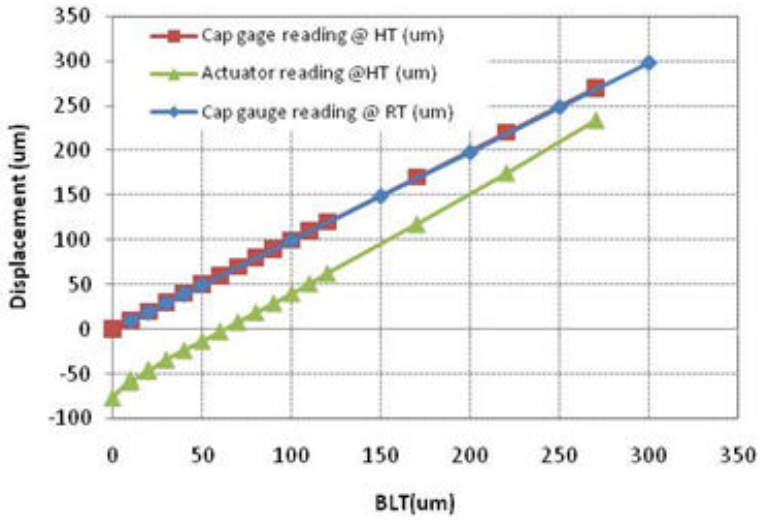

Figure 15. Cap gage and actuator calibration plot at high temperature (110°C).

3.1.3 Accuracy Evaluation

Measurement capability analysis (MCA), a statistical process for evaluating metrology capability, was performed using thermal grease as testing material. Typical MCA consists of static repeatability, dynamic repeatability and dynamic reproducibility of the measurements to assess the capability of the metrology for required measurement.

For MCA, thermal grease was selected for its good thermal performance and the pump-out issues. Since thermal grease can pump-out easily during testing, it was considered as a “worst” case material in terms of repeatability of measurements. Therefore, dynamic repeatability MCA was performed as it includes all noise factors from measurement and closely mimics the actual testing scenario.

A total of 6 measurements were collected for thermal grease under 20, 50 and 90 psi pressure. For each test, rods were engaged and the cap gauge was zeroed out. The rods were separated and thermal grease was dispensed between the rods. Rods were then engaged and heaters were powered so that the material temperature was approximately 90°C. Pressure was applied to the sample, initially 20 then 50 and finally 90 psi. Time was allowed at each pressure for steady state to be reached. Measurements of temperature, power, bond line thickness (BLT) and load were continuously taken during entire test time. With the test completed, rods were cleaned. New thermal grease samples were dispensed between the rods and the process was repeated. Figure 16 through Figure 19 show MCA results for BLT, thermal resistance, thermal impedance, and effective thermal conductivity, respectively. In addition results for each parameter are summarized in Table 2 through 5 below the figures.

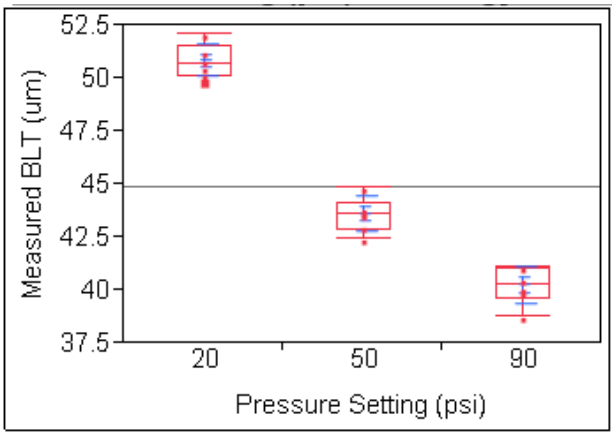

Figure 16. MCA results for measured BLT – dynamic repeatability study.

Table 2. Summary of MCA results for measured BLT - dynamic repeatability study.

Pressure	Number of Measurements	Mean	Std Dev	Std Err Mean	Lower 95%	Upper 95%
20	6	50.81	0.7583	0.3096	50.02	51.61
50	6	43.56	0.8209	0.3351	42.70	44.42
90	6	40.22	0.8708	0.3555	39.30	41.13

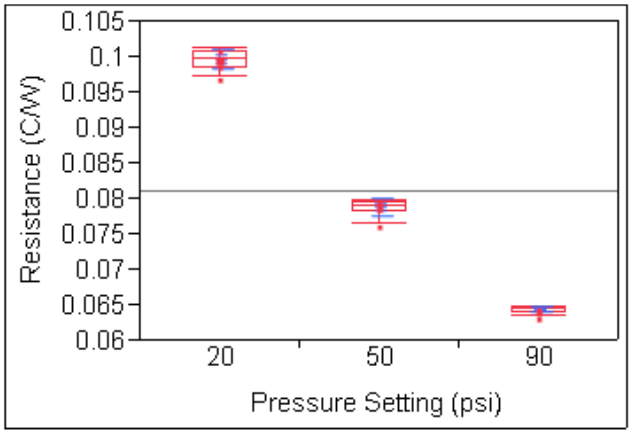

Figure 17. MCA results for thermal resistance – dynamic repeatability study.

Table 3. Summary of MCA results for thermal resistance – dynamic repeatability study.

Pressure	Number of Measurements	Mean	Std Dev	Std Err Mean	Lower 95%	Upper 95%
20	6	0.0996	0.0014	0.0006	0.0982	0.1010
50	6	0.0788	0.0012	0.0005	0.0775	0.0800
90	6	0.0644	0.0004	0.0002	0.0639	0.0648

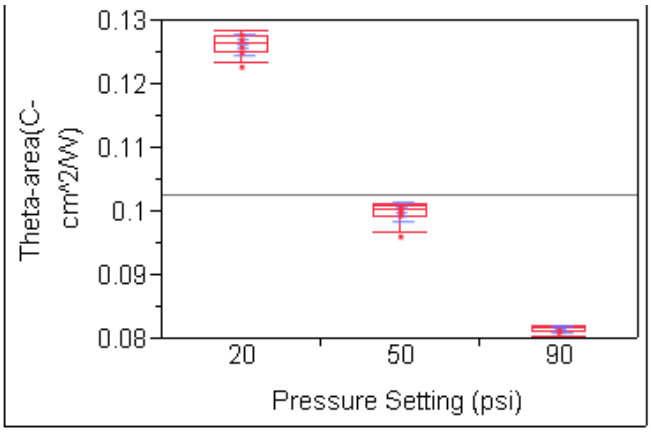

Figure 18. MCA results for thermal impedance – dynamic repeatability study.

Table 4. Summary of MCA results for thermal impedance – dynamic repeatability study.

Pressure	Number of Measurements	Mean	Std Dev	Std Err Mean	Lower 95%	Upper 95%
20	6	0.1262	0.0017	0.0007	0.1244	0.1280
50	6	0.0998	0.0015	0.0006	0.0982	0.1014
90	6	0.0815	0.0005	0.0002	0.0809	0.0820

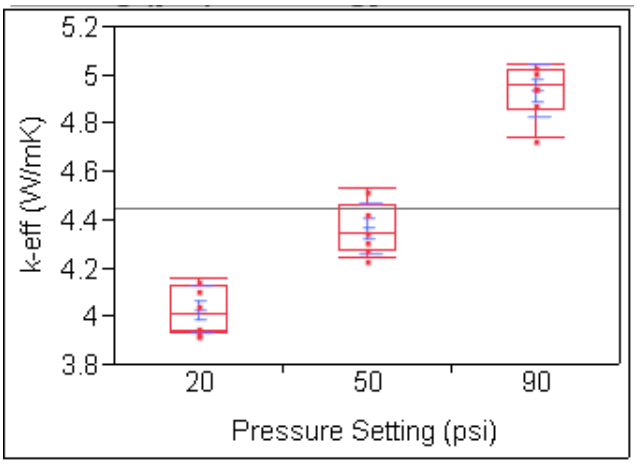

Figure 19. MCA results for effective thermal conductivity – dynamic repeatability study.

Table 5. Summary of MCA results for effective thermal conductivity – dynamic repeatability study.

Pressure	Number of Measurements	Mean	Std Dev	Std Err Mean	Lower 95%	Upper 95%
20	6	4.0271	0.0972	0.0397	3.9251	4.1290
50	6	4.3653	0.1048	0.0428	4.2553	4.4753
90	6	4.9359	0.1072	0.0438	4.8234	5.0484

The overall summary of the MCA results is tabulated in Table 6. The results show highly repeatable measurements with low standard deviations for all metrics. Three sigma (3σ), i.e. 3*standard deviation, was calculated for each metric at each applied pressure and is listed in the table. The 3σ values will be used as error bounds for the design of experiments (DOE) measurements.

Table 6. Overall Summary of MCA results for Angular TIM Tester.

Metric	Pressure (psi)	Mean	Std Dev	3 Sigma
BLT (um)	20	50.81	0.7583	2.2750
	50	43.56	0.8209	2.4628
	90	40.22	0.8708	2.6123
Thermal Resistance ($°C\ W^{-1}$)	20	0.0996	0.0014	0.0041
	50	0.0788	0.0012	0.0036
	90	0.0644	0.0004	0.0013
Thermal Impedance ($°C\ cm^2\ W^{-1}$)	20	0.1262	0.0017	0.0051
	50	0.0998	0.0015	0.0046
	90	0.0815	0.0005	0.0016
Effective Thermal Conductivity ($W\ m^{-1}\ K^{-1}$)	20	4.0271	0.0972	0.2915
	50	4.3653	0.1048	0.3145
	90	4.9359	0.1072	0.3216

3.2 Bare Die Tilting Metrology

The design of the Bare Die Tilting Metrology is very similar to that of the Mini Angular TIM Tester with the difference of using a bare die package instead of copper rods for testing. The overall dimensions of the

metrology are 14x12x22 inches. As with the TIM tester, the metrology is aligned using high precision bearings, x-y and tilt stages allowing for precise alignment. Once again, the tilt stage is used to perform testing under a specific tilt angle. For this metrology, a pneumatic cylinder with pressure/load control is used to engage the cooling solution, cold block, and the electronic package and provide adequate mechanical loading to the package. The metrology is depicted in Figure 20.

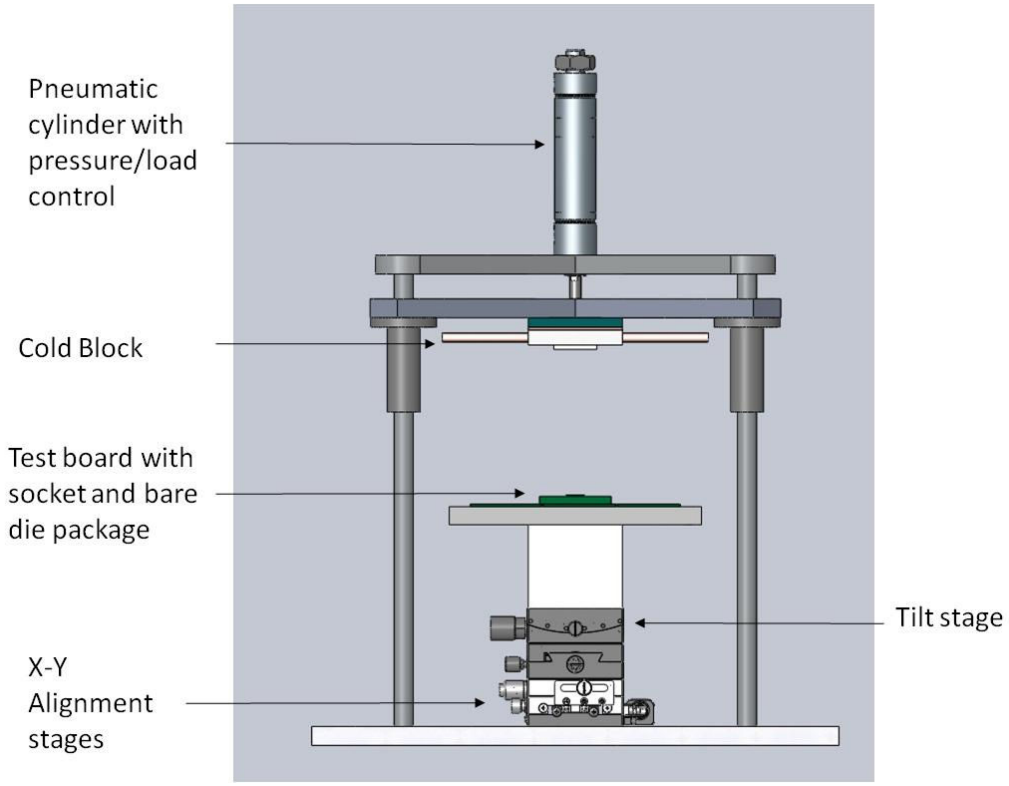

Figure 20. Bare Die Tilting Metrology.

The goniometer on the tilt stage is used for precise angle measurement. It is important to indicate that the setup was designed so

that the pivot point was located at the top center of the die to prevent any horizontal translation during measurements under applied tilt angle.

A pedestal cold block, whose temperature is controlled by a chiller, is used to provide cooling to the electronic package. One k-type thermocouple is embedded into the center of the cold block pedestal. The size of the pedestal is slightly larger than the overall size of the die. The schematic of the cold block with the position of the thermocouple is illustrated in Figure 21.

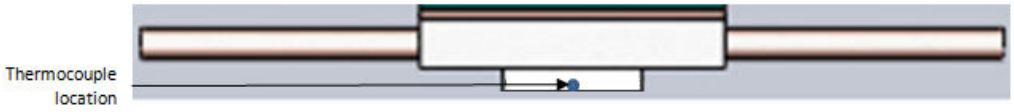

Figure 21. Thermocouple location in cold block.

Figure 22 shows the front view schematic of a bare die electronic package. As shown in Figure 22, the silicon die is connected via C4 bumps, (solder bumps that have been deposited onto the chip pads), to the organic substrate. For structure rigidity, the polymer underfill is used to fill the space between the C4 bumps. A pin grid array (PGA) socket mounted to the enabling test board (ETB) is used for mounting the electronic package. The ETB then provides the means for electrical connection between the package and data acquisition for the required thermal measurements.

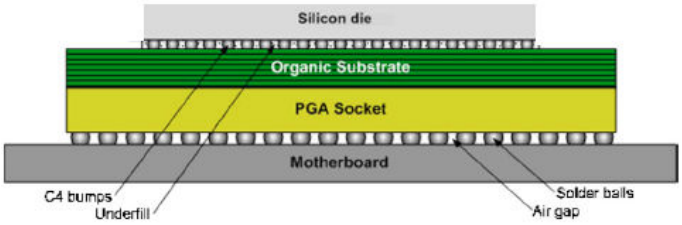

Figure 22. Electronic package schematic.

In the current study a thermal test vehicle (TTV) which closely represents an electronic package was used for measurements. The TTV has a uniform heater on the silicon die and several thermal sensors for temperature measurements. The thermal sensors on the TTV, called resistance temperature devices or RTDs, have linear electrical resistance to temperature relationship within the temperature range used in the current study.

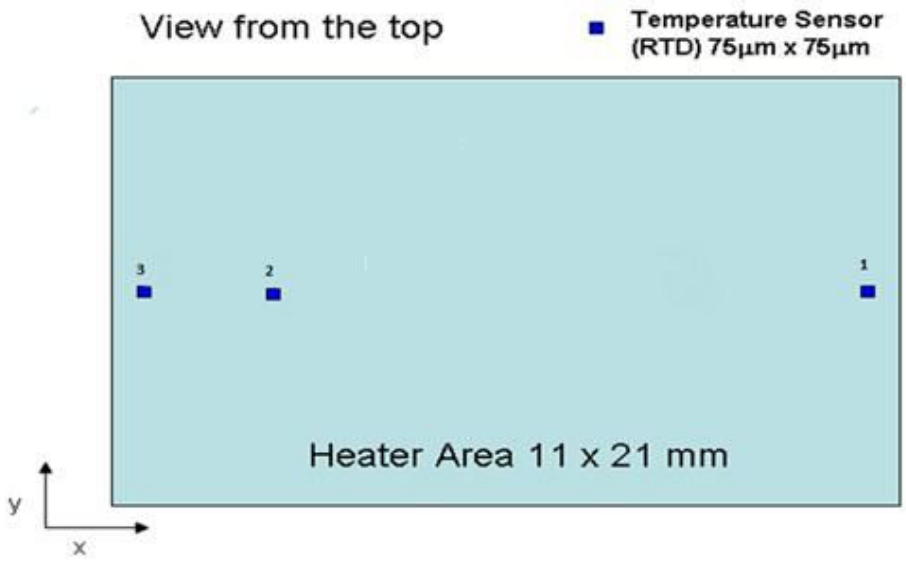

Figure 23. TTV schematic with location of the RTDs with uniform heater covering 11 x 21 mm area.

The cross section of the TTV package schematic with the location of the RTDs is shown in Figure 23. The uniform heater covers 11 by 21 mm area of the die. Three temperature sensors were fabricated on the heat-generating die to adequately measure the junction temperature of the bare die package. The die has copper interconnect layers on the surface of the bulk silicon substrate in which the heater and RTDs are located.

The main heater has serpentine structure and is uniformly distributed across the die in 11 mm by 21 mm area with line width and pitch on the order of a few microns. The RTDs are also fabricated on the metal layer and their location is illustrated in Figure 25. The three RTDs are located along the x-axis in the center of the package with RTD 1 at the high and RTD 3 at the low edge of the package. The location of RTD 2 is at the pivot point as will be discussed later in the results section.

Finally, the data acquisition (DAQ) system, which includes Agilent E8401A VXI Mainframe, Agilent 6030A 0-200V/0-17A power supply, Agilent E1586A and VT1586A terminal panels, is used to power the heater, measure the resistance of the RTDs on the TTV and measure the cold block thermocouple temperature.

3.2.2 Metrology Calibration

To obtain accurate results from the metrology it is essential to calibrate the RTDs. For precise die temperature measurements, the RTDs were initially calibrated in an isothermal bath at five different

temperatures. The relationship between the electrical resistance and temperature was obtained and applied to get the die junction temperature measurement. A typical RTD calibration curve is illustrated in Figure 24.

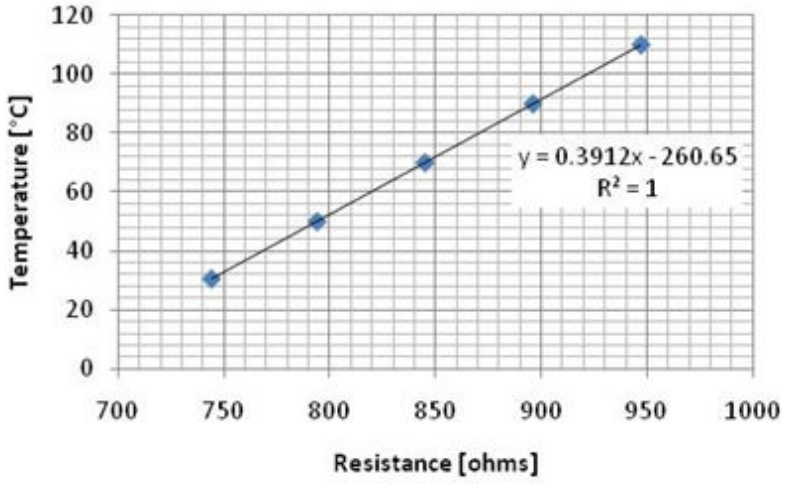

Figure 24. Representative RTD calibration curve.

3.2.3 Accuracy Evaluation

Metrology validation was completed by a dynamic repeatability study. Thermal grease was used as the thermal interface between the bare die and the cold block. Six measurements were completed at 0° and 0.5° tilt angles. Grease was reapplied between each measurement. The angle of tilt was verified using TekScan™ and digital protractor. The tilt was applied over the y-axis as indicated in Figure 25 for all measurements.

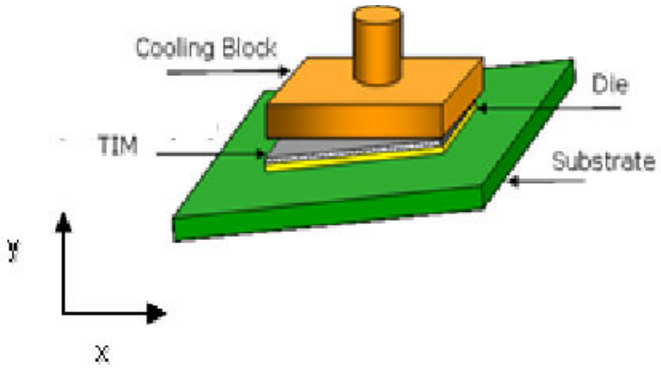

Figure 25. TTV and cold block schematic indicating the direction of the tilt.

The metrology was validated by examining the change in thermal resistance between the die junction and cold block temperature with the change in tilt angle. Thermal resistance between junction and cold block is defined by Equation (15):

$$\theta_{jp} = \frac{\Delta T}{P} \tag{15}$$

where P is the total power in [W] applied to the die and $\Delta T = T_j - T_p$ is the temperature difference between the junction temperature T_j and cold block or plate temperature T_p, both in [°C]. Then the change in thermal resistance with change in tilt angle can be defined by

$$\Delta\theta_{jp} = \theta_{jp@angle} - \theta_{jp@0} \tag{16}$$

Where $\theta_{jp@angle}$ is the thermal resistance at a specific angle and $\theta_{jp@0}$ is the thermal resistance at 0° tilt.

The metrology was validated by performing dynamic reproducibility MCA. Unit was placed into the socket, thermal grease was dispensed and cold block was engaged. Unit was powered and data was collected at steady state. The criterion for steady state was +/- 0.2°C change in

temperature over a period of 5 minutes. The MCA results are presented in Figure 26 for all three sensors as discussed previously. The importance of the MCA is the standard deviations, i.e. the metrology dynamic repeatability capability. Once again the 3σ values will be used as error bounds for the DOE measurements. Data are summarized in Table 7.

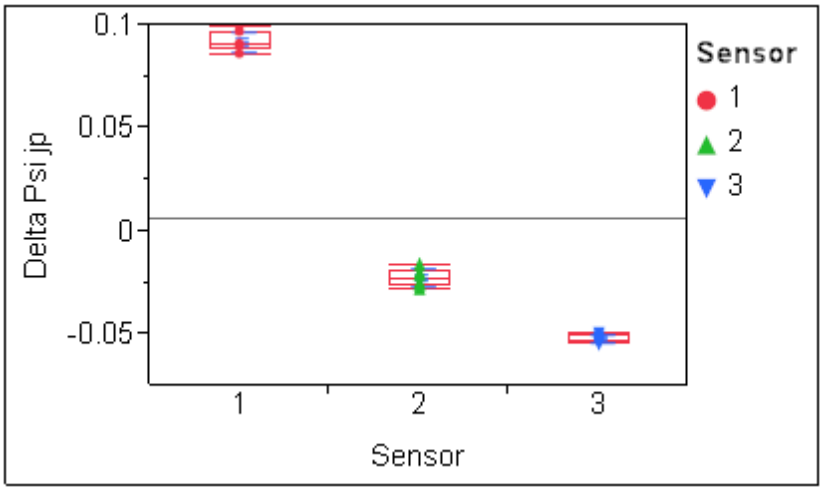

Figure 26. Bare Die Tilting Metrology MCA results.

Table 7. MCA results summary for Bare Die Tilting metrology.

Sensor	Mean	Std Dev	3 Sigma
1	0.09157	0.00490	0.01471
2	-0.02301	0.00434	0.01301
3	-0.05276	0.00188	0.00565

Chapter 4

RESULTS AND DISCUSSION

Three different types of TIMs were selected for measurements, namely thermal grease, phase change material and gap filler. Each material was selected based on their characteristics, wide range of usage and thermal performance.

Two types of thermal grease and phase change TIM were selected primarily based on the fact that they are most commonly used TIM. In addition, due to their paste characteristic, thermal greases and PCMs have good surface wetting capability generally resulting in low contact resistance. Low bond line thickness can be achieved with these TIMs and hence they have good thermal performance. It was important to study the ability of these materials to conform to tilted surfaces and understand the effect of the tilt to their performance.

The primary usage of gap fillers is to fill in large gaps between two surfaces in contact. Therefore, two different gap fillers were selected to study their ability to fill in induced tilt angles. Three different preform thicknesses, 0.5, 1.0 and 3.0 mm, of each material were tested. Selected TIM specifications are summarized in Table 8.

Table 8. Summary of selected TIMs specifications.

	Thermal Grease Type 1	Thermal Grease Type 2	Phase Change TIM	Gap Filler TIM Type 1	Gap Filler TIM Type 2
Appearance	Gray	White	Gray	Gray	Gray
Specific Gravity (25C)	2.5	3.3	2.4		
Thermal Conductivity (W/mK)	4.5	3.02	3	4.5	3

All of the materials were tested in both metrologies described in Chapter 3.

4.1 Angular TIM Tester Results and Discussion

The first set of experiments were performed on the Angular TIM tester (Figure 12). The experimental procedure was kept the same between the TIMs. Initially, rods were engaged to 20 psi and the capacitance gauge was zeroed out. TIM was then dispensed between the rods, rods were engaged and heat was applied. The applied power, in W, depended on the type of material under test. The power was tuned until ~ 90°C TIM temperature was reached. The chiller temperature was always kept at 23°C (room temperature). Tests were performed at 20, 50 and 90 psi pressure for each TIM ensuring steady-state temperature was reached at each pressure. Once again the criterion for steady state was +/- 0.2°C temperature change over 5 minutes period.

First, all TIMs were tested at 0° tilt and then the process was repeated at 0.3° and 0.6° tilt angle. The tilt angles were chosen based on the preliminary testing results on a bare die package. It was found that at 0.6° tilt angle all load is applied to the very edge of the die and 0.3° tilt was a midpoint. This reasoning will be clearer in discussion of Bare Die Tilting Metrology results presented in section 4.2

4.1.1 Thermal Grease

Results for two thermal greases tested at 0° tilt angle are shown in Figure 27. As expected, the thermal impedance (i.e. thermal resistance times cross sectional area) decreases with the increase in applied pressure. The increase in pressure reduces the BLT of the TIM as well as the contact resistance. For that reason the overall thermal resistance of the TIM decreases with increase in pressure. As evident from the figure, type 1 thermal grease had a lower overall thermal resistance as compared to type 2 grease. This was also expected as the bulk thermal conductivity of type 1 grease is ~4.5 W/mK while the bulk thermal conductivity of type 2 grease is ~ 3 W/mK as outlined in Table 8.

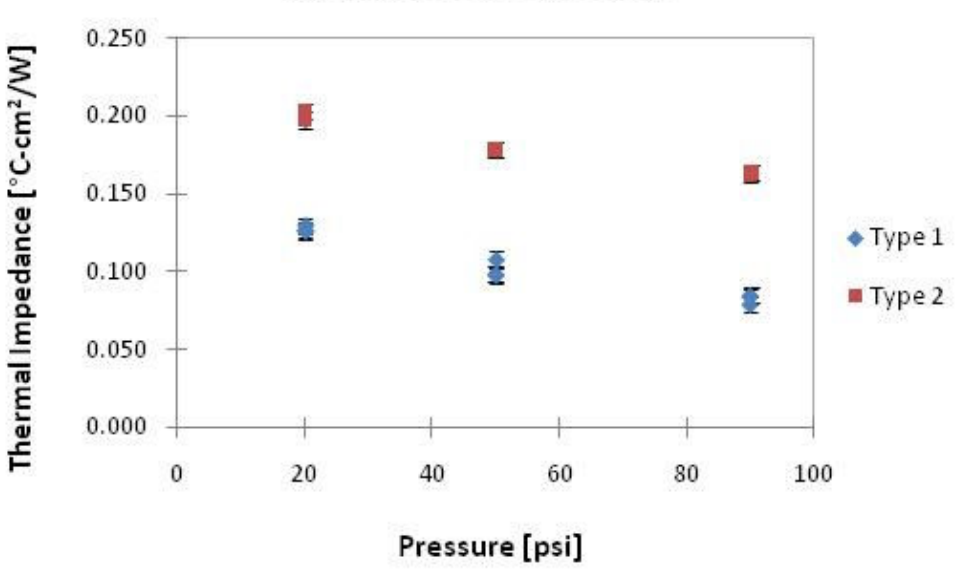

Figure 27. Thermal grease results at 0° tilt angle.

The results for thermal impedance vs. pressure at 0.3° and 0.6° tilt for the two greases are summarized in Figures 28 and 29. Same as at 0°,

the thermal impedance at these two angles decreases with the increase in pressure.

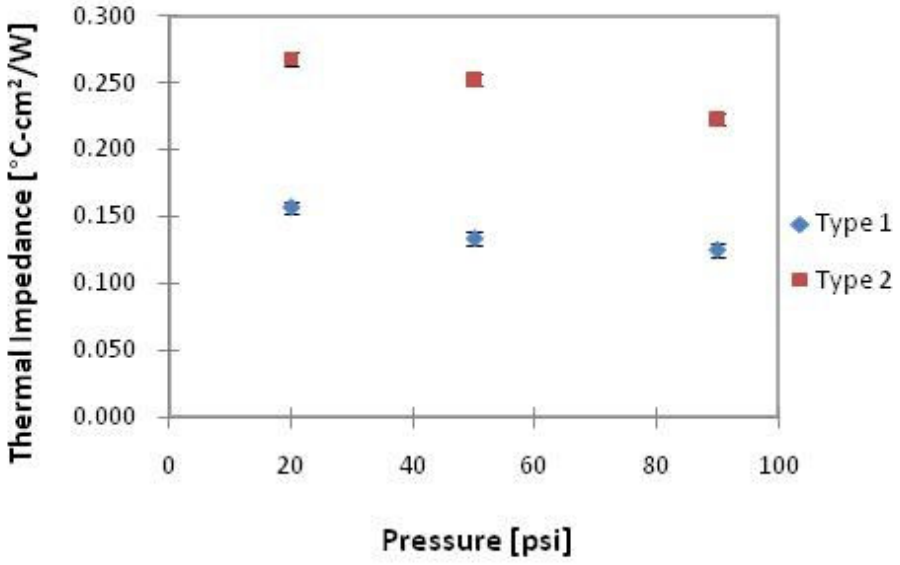

Figure 28. Thermal grease results at 0.3 tilt angle.

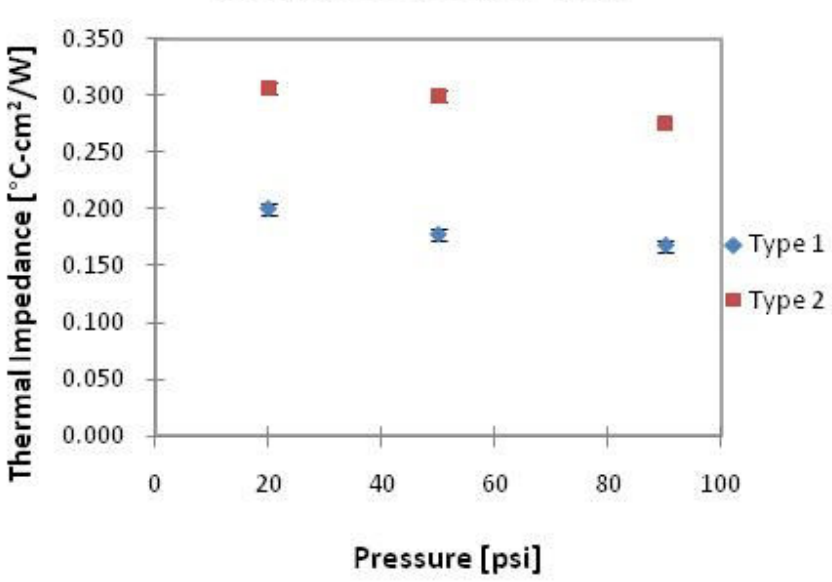

Figure 29. Thermal grease results at 0.6 tilt angle.

Figure 30 shows results for thermal impedance vs. tilt angle for thermal grease type 1. As the angle of tilt increases so does the thermal impedance. This indicates that for thermal grease, contact resistance increases with tilt angle.

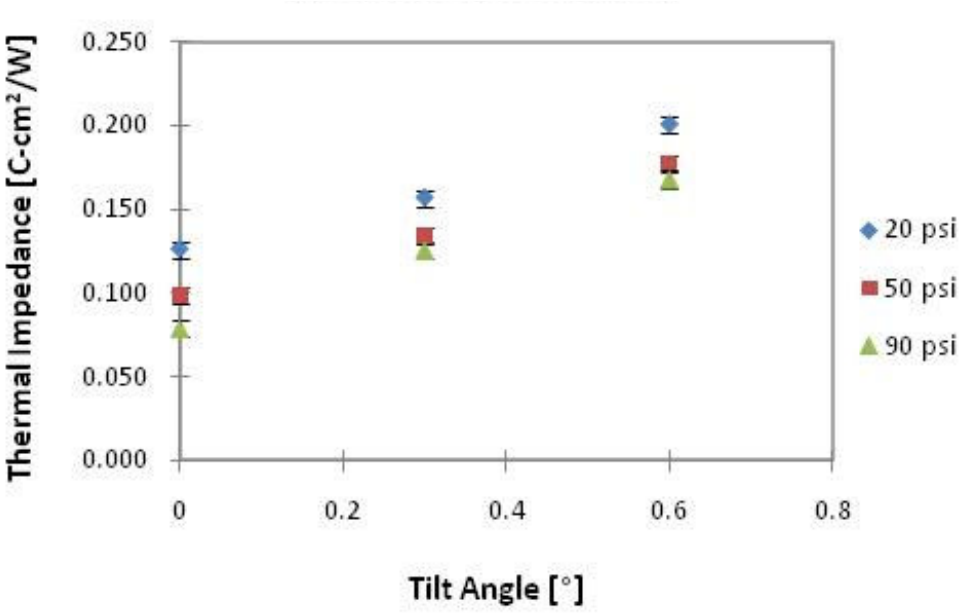

Figure 30. Type 1 thermal grease resistance change vs. tilt angle.

The loading pressure also changes with the change in tilt angle. TekScan™ images were taken for the pressure and contact between the rods at each tilt angle. The images were taken between bare rods i.e. no TIM. The above results are summarized once again highlighting the contact pressure change with the tilt change between the rods and presented in Figure 31.

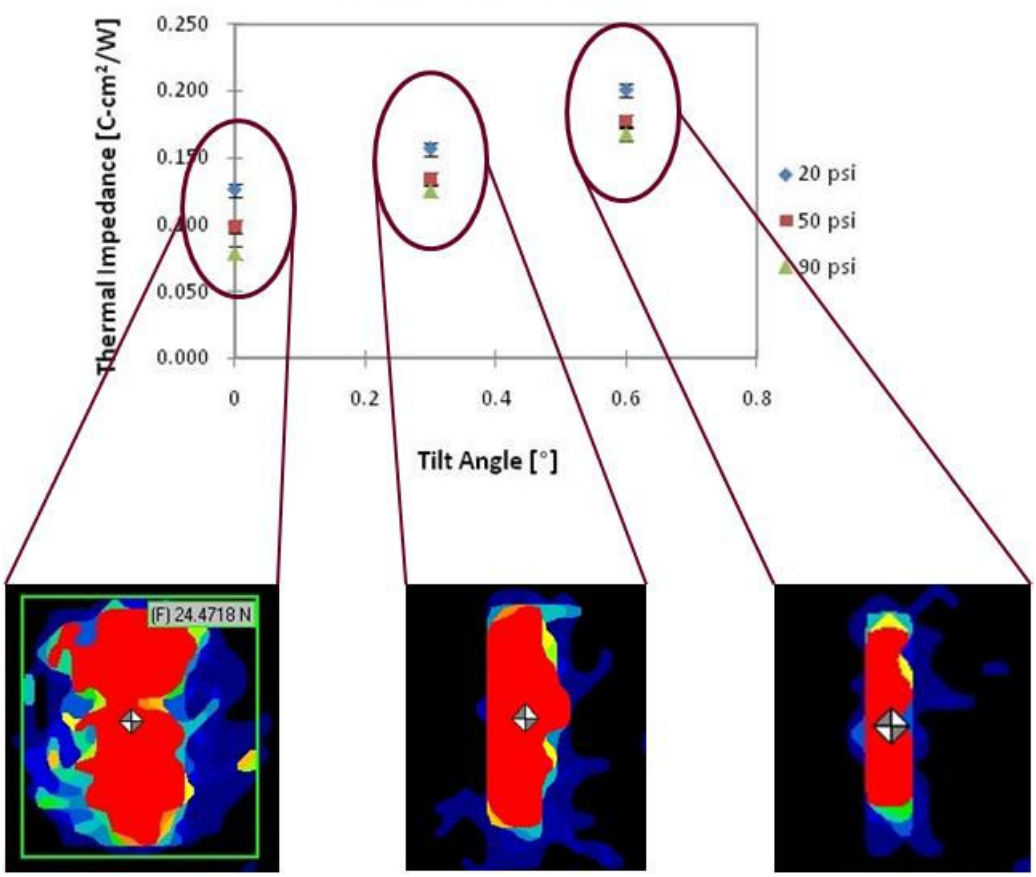

Figure 31. Impact of tilt angle on rods contact.

Figure 32 summarizes the results of thermal impedance change vs. tilt angle for thermal grease type 2. The impact on thermal impedance is the same as for that of thermal grease type 1. This is expected as both materials have similar characteristics. In summary, tilt angle shows a significant impact on thermal grease performance in the Angular TIM tester.

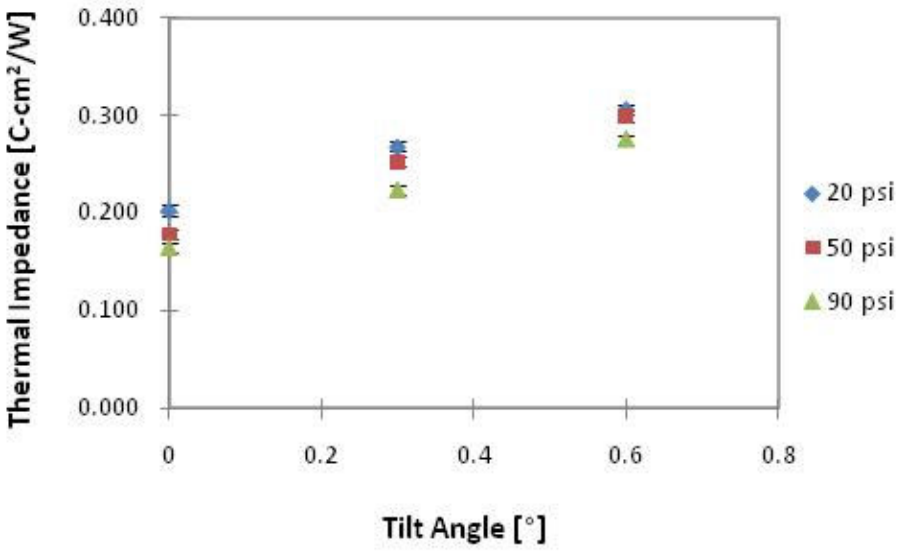

Figure 32. Type 2 thermal grease resistance change vs. tilt angle.

4.1.2 Phase Change TIM

Next, PCM data was collected using the same procedure as described for thermal grease above. The results for thermal impedance vs. tilt angle are shown in Figure 33.

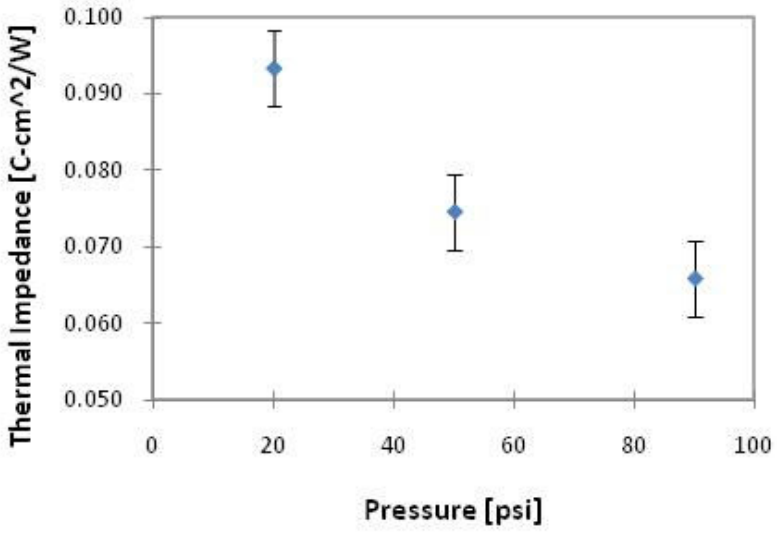

Figure 33. Phase change TIM results at no tilt angle.

It is evident from the data in Figure 33 that the thermal impedance decreases with the increase in applied pressure. As the behavior of PCM is similar to thermal grease above its phase change temperature (for this material ~70°C), the results are as expected.

The same response is evident for data collected at 0.3° and 0.6° angles. The thermal impedance decreases with an increase in pressure at all angles tested. A summary of the results at 0.3° and 0.6° are presented in Figures 34 and 35.

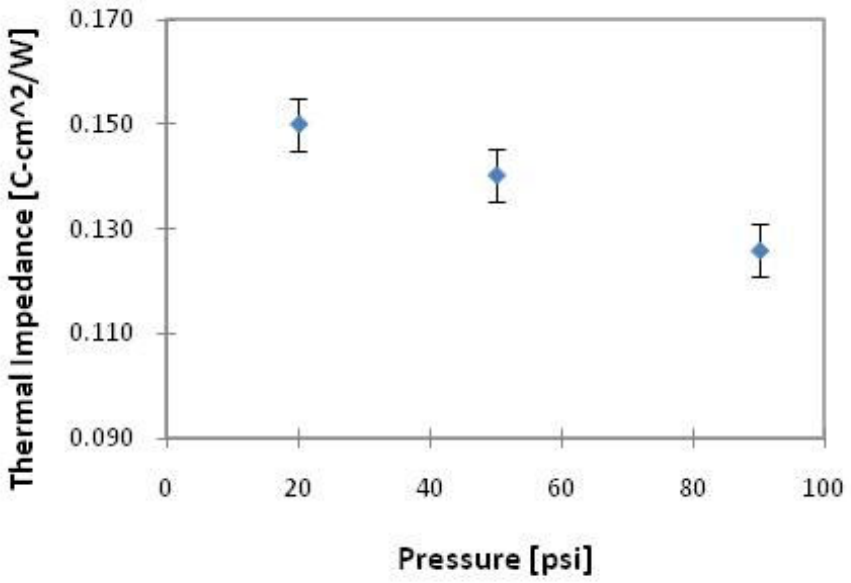

Figure 34. Phase change TIM results at 0.3 tilt angle.

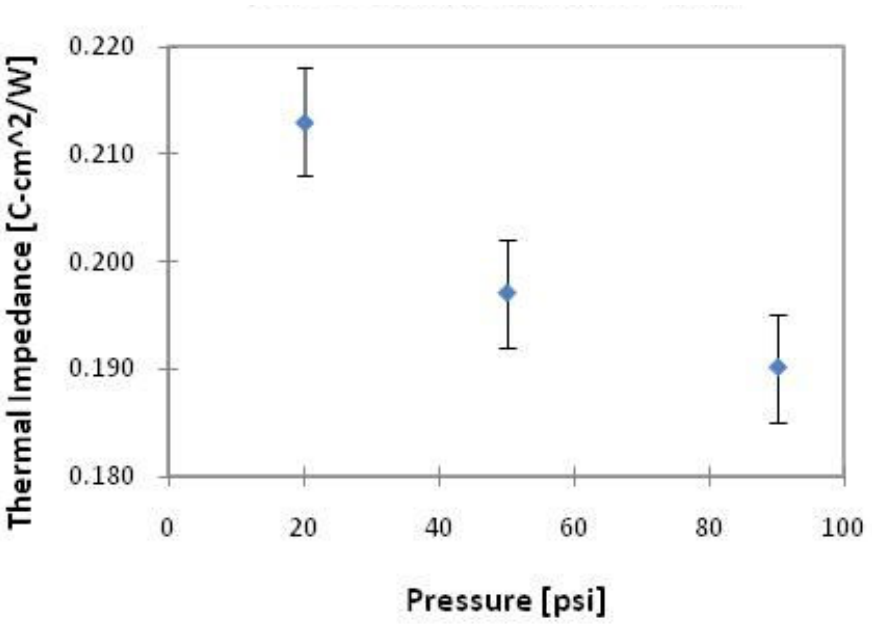

Figure 35. Phase change TIM results at 0.6 tilt angle.

Next, thermal impedance vs. tilt angle was plotted for the PCM and the results are presented in Figure 36. Once again, thermal impedance increases with the increase in tilt angle at all pressures. As for the thermal grease, it is evident that the angle of tilt impacts the thermal performance of the PCM.

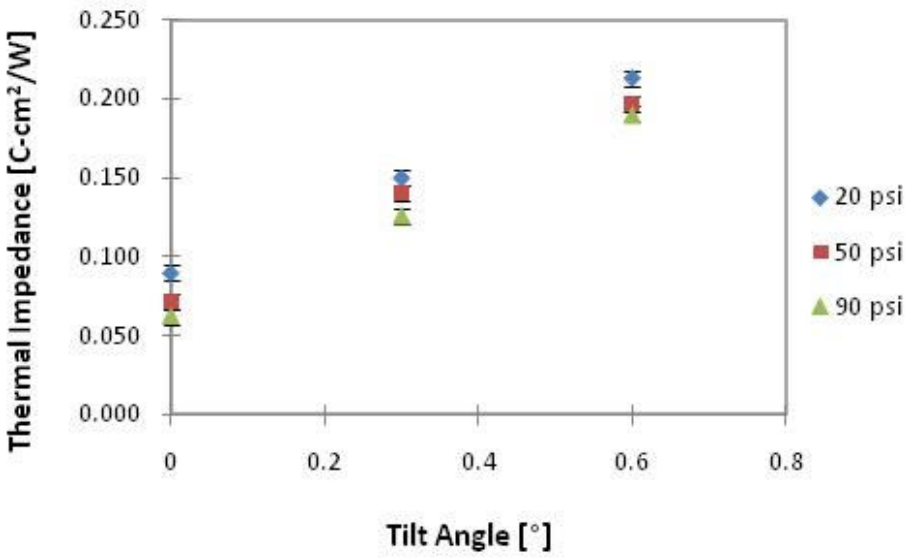

Figure 36. Phase change TIM resistance vs. tilt angle.

4.1.3 Gap Fillers

Finally, data were collected on the two gap fillers following the same procedure. Results for type 1 gap filler, thermal impedance vs. pressure for all three perform thicknesses at 0°, 0.3° and 0.6° tilt angles are summarized in Figures 37, 38 and 39 respectively.

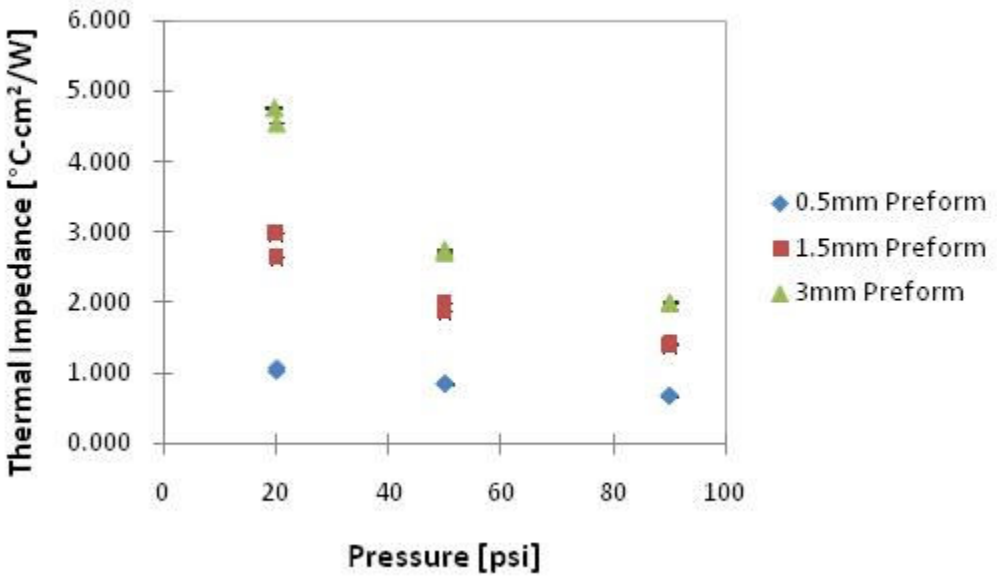

Figure 37. Type 1 gap filler results at no tilt.

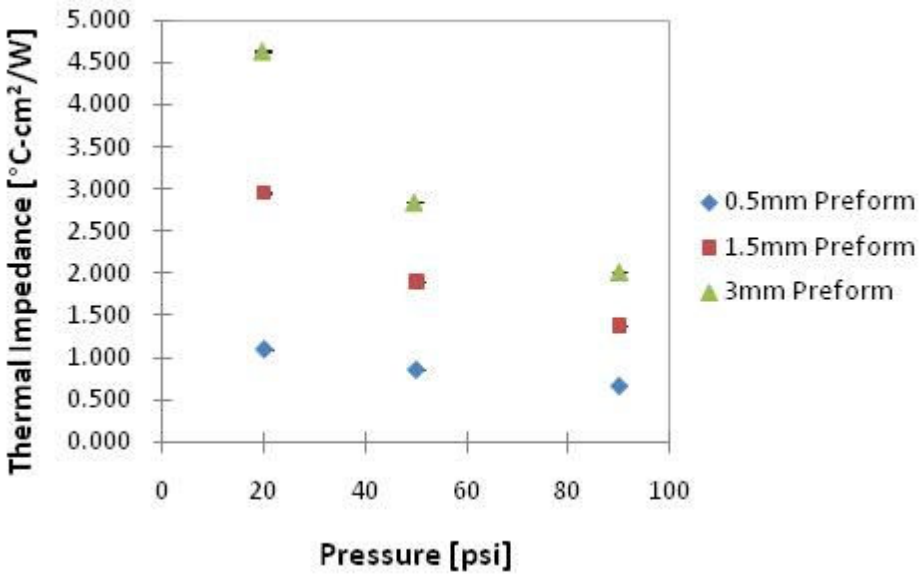

Figure 38. Type 1 gap filler results at 0.3 tilt angle.

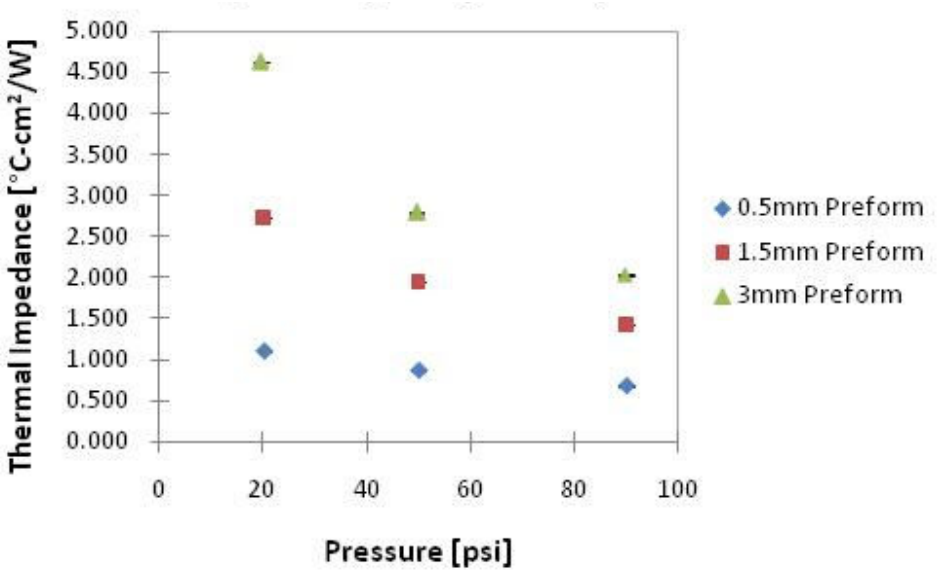

Figure 39. Type 1 gap filler results at 0.6 tilt angle.

From the above three figures it is evident that the thermal performance of the gap filler highly depends on its preform thickness, and applied pressure at all angles. The impact of pressure on the thermal performance of gap fillers increases with the increase in preform thickness of the TIM. For example, it was found that the percent difference for 3-mm preform thickness from 20 to 50 psi was ~ 40%, for 1.5-mm preform ~ 25%, and for 0.5-mm preform ~ 18%. Therefore, the applied pressure is a significant factor in the gap filler performance and higher loads should be applied to thicker TIM performs where possible.

Next, the results for gap filler type 1, thermal impedance vs. tilt angle for each of the three preform thicknesses are plotted in Figures 40, 41 and 42 respectively.

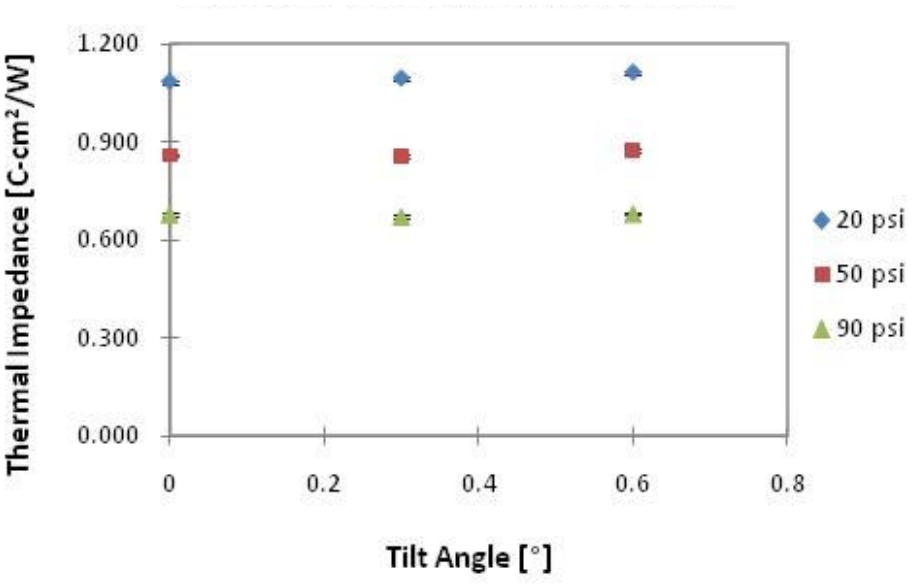

Figure 40. Type 1 0.5-mm preform gap filler resistance vs. tilt angle.

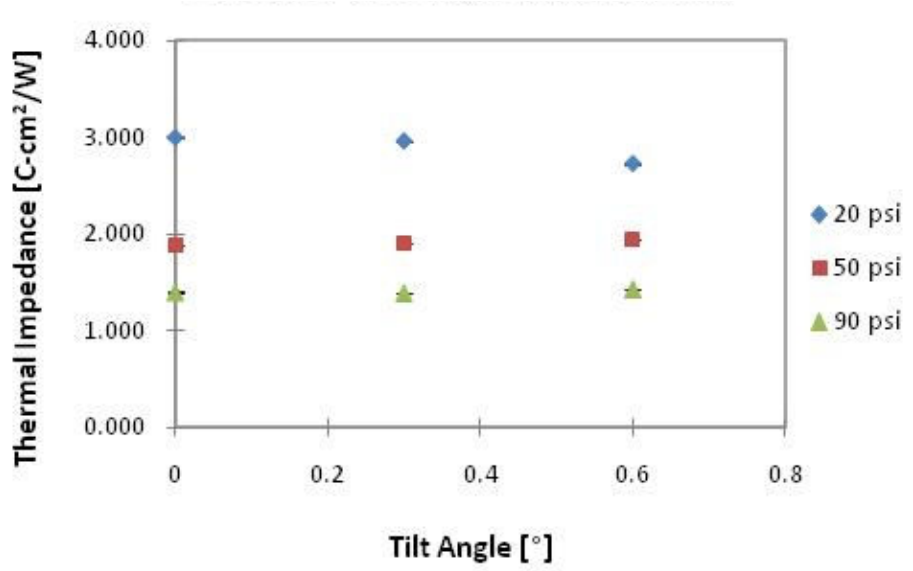

Figure 41. Type 1 1.5-mm preform gap filler resistance vs. tilt angle.

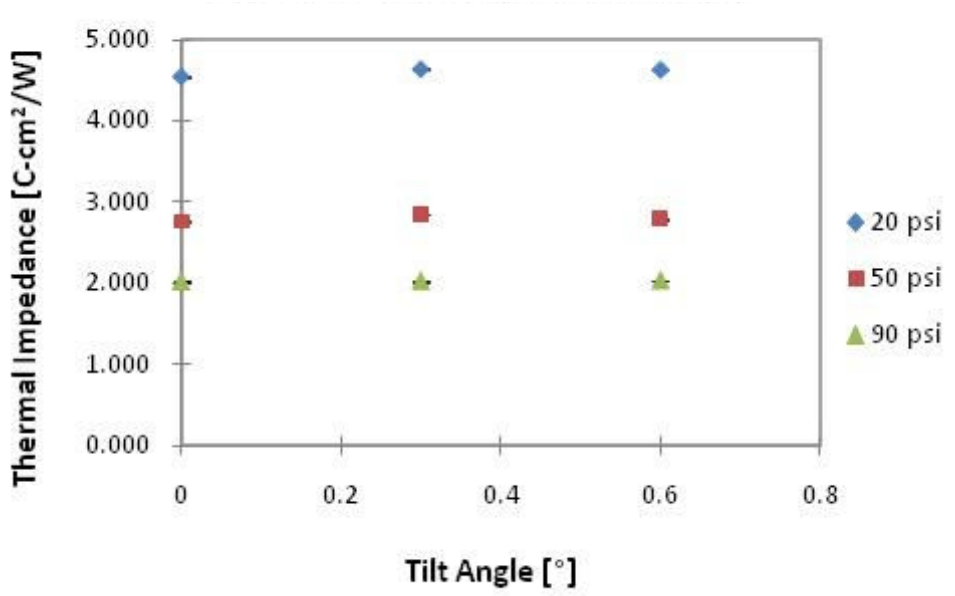

Figure 42. Type 1 3-mm preform gap filler resistance vs. tilt angle.

As evident from Figure 40 through 42, tilt angle does not seem to have a significant impact on thermal impedance. At each pressure, and for each preform thickness, no significant change in thermal performance is observed with the increase in tilt angle. The results suggest that gap filler preform thickness and pressure play bigger roles in the performance of the material then does a gap/tilt applied between two mating surfaces.

Gap filler type 2 results are depicted in Figures 43, 44 and 46 for thermal impedance vs. tilt angle. Results for type 2 gap filler have the same trends as those of type 1. Applied pressure plays a significant role in the thermal performance of this material with higher impact on thicker material preform.

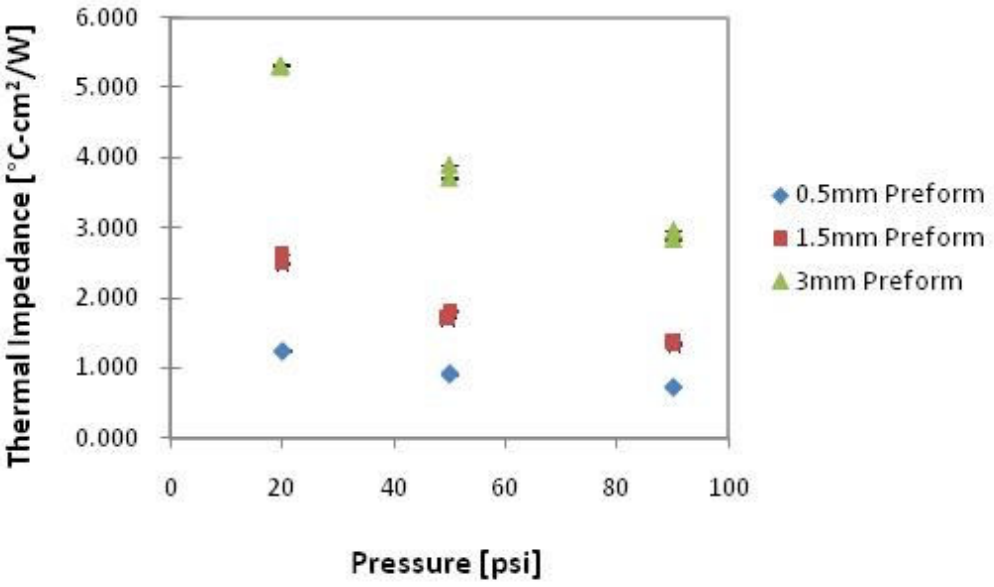

Figure 43. Type 2 gap filler results at no tilt angle.

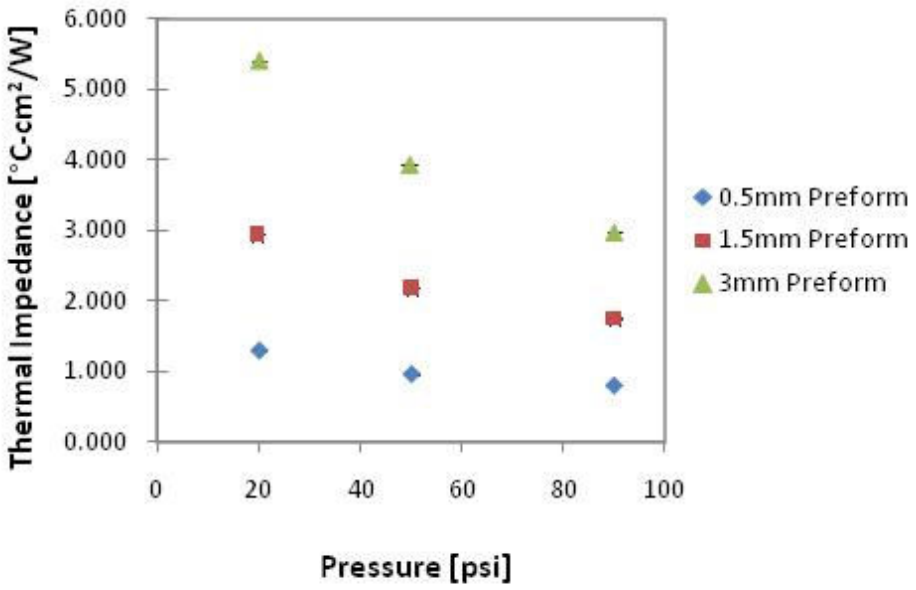

Figure 44. Type 2 gap filler results at 0.3 tilt angle.

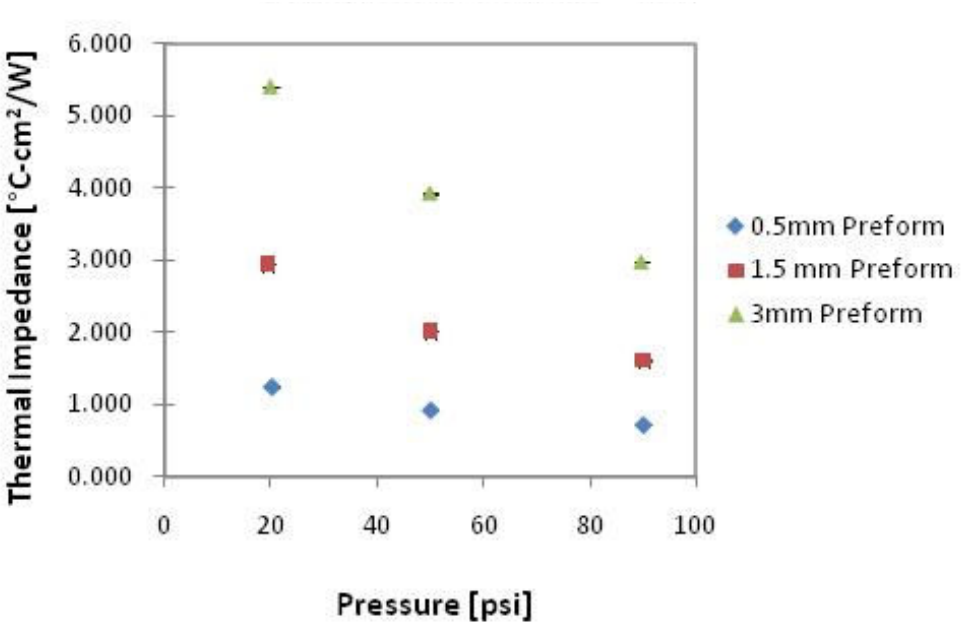

Figure 45. Type 2 gap filler results at 0.6 tilt angle.

Finally, the results of thermal impedance vs. tilt angle for all three preform thicknesses of gap filler type 2 are plotted in Figures 46 through 48. Once again, the angle of tilt within the range tested, seems to have no significant impact on this material's thermal performance.

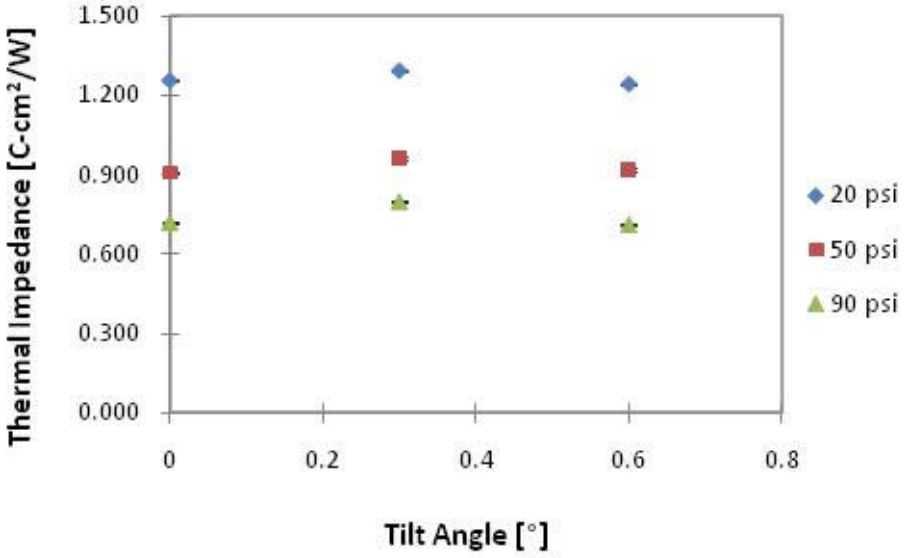

Figure 46. Type 2 0.5-mm preform gap filler resistance vs. tilt angle.

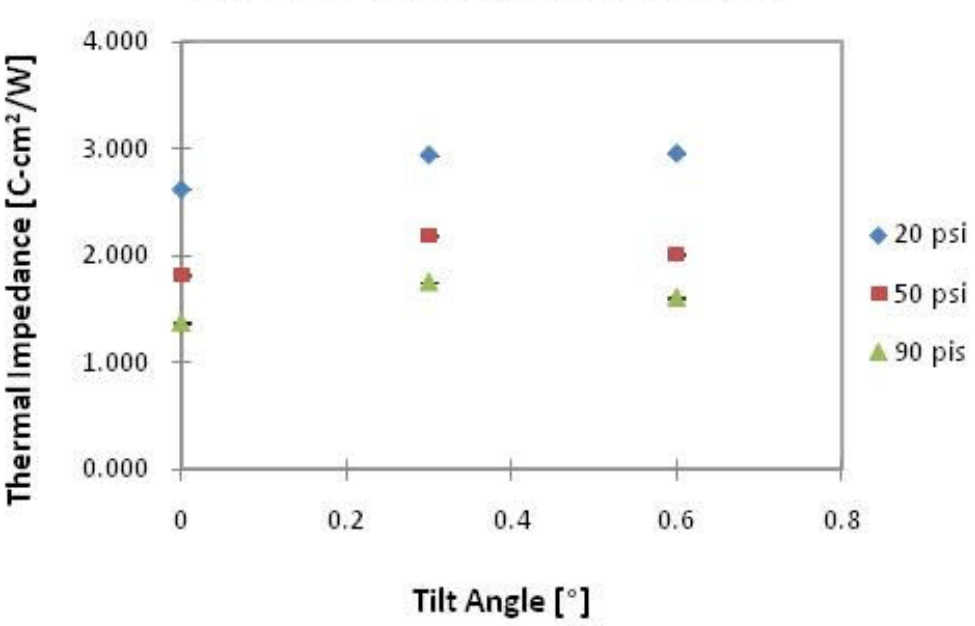

Figure 47. Type 2 1.5-mm preform gap filler resistance vs. tilt angle.

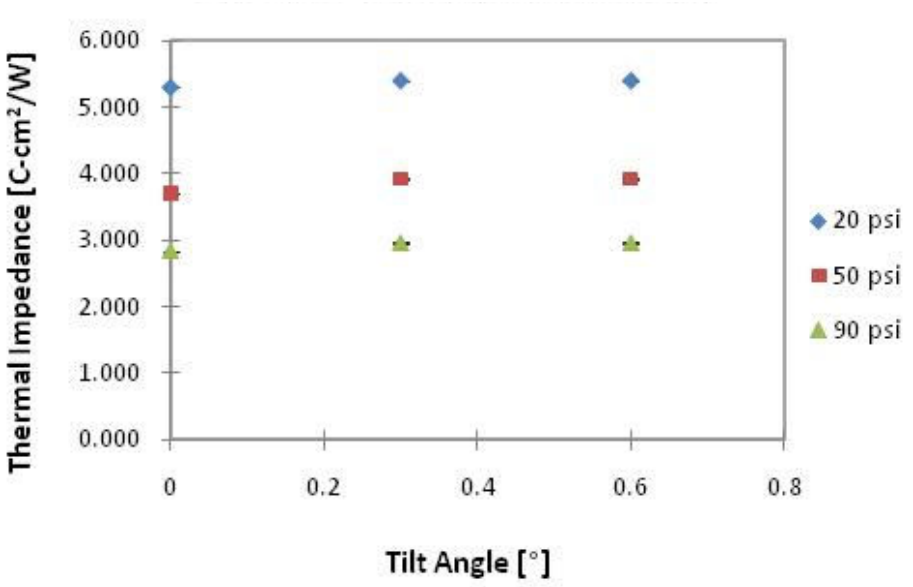

Figure 48. Type 2 3-mm preform gap filler resistance vs. tilt angle**.**

4.2 Bare Die Tilting Metrology Results and Discussion

As discussed earlier, Bare Die Tilting metrology was developed to characterize the selected materials in-situ, i.e., in actual applications. Constant loading was applied for all TIMs, and applied power was varied in dependence of the TIM such that the package junction temperature at steady state was ~ 90°C for all of the TIMs. Each TIM was measured at 0°, 0.3° and 0.6° tilt between the bare die package and the cooling solution. Figure 49 shows a schematic of contact area/pressure between the bare die and the cooling solution for all three angles of test.

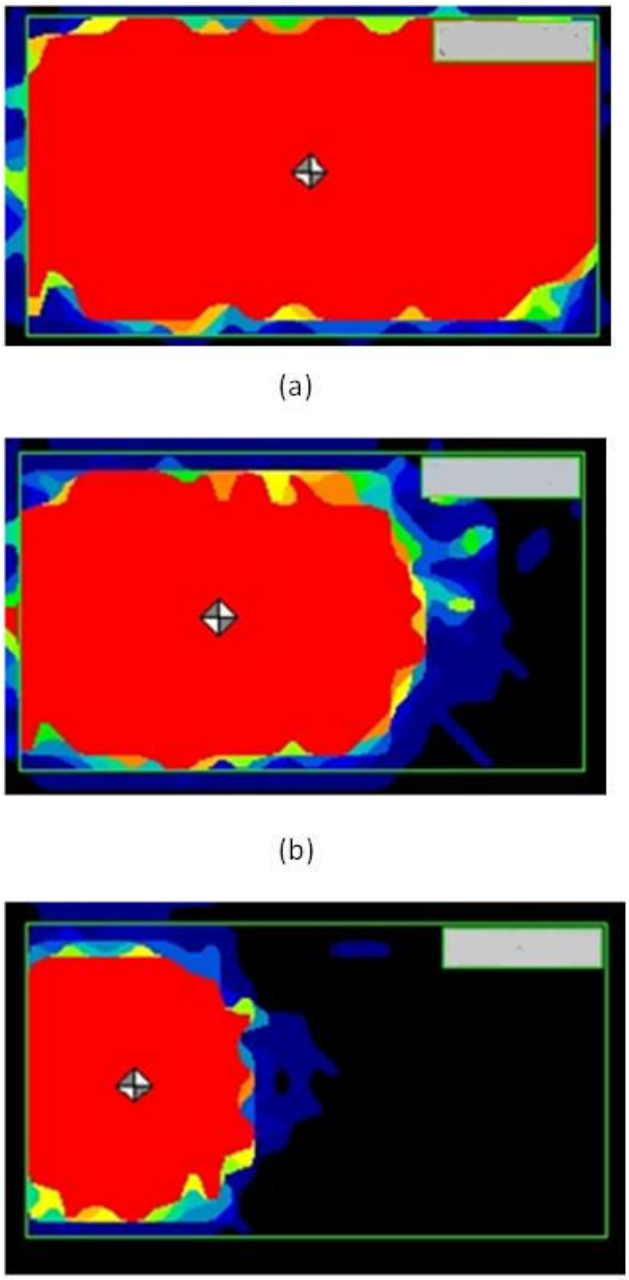

Figure 49. Pressure/contact profile of die and cooling solution at (a) 0° tilt angle; (b) 0.3° tilt angle; (c) 0.6° tilt angle

4.2.1 Dry Contact

For reference purposes, initial measurements were conducted for a dry contact, i.e., no TIM was applied between the bare die and the cooling solution. The experimental results for Sensors 1, 2 and 3 are summarized in Figures 50. As a reminder, the sensor 1, 2 and 3 are RTDs located on the bare die at positions high edge, off-center, and low edge as illustrated in Figure 50.

Results for dry contact show a worst case scenario impact of tilt angle to thermal performance of the bare die package. They can also be used as evidence of the importance of the TIM material for the electronic package performance.

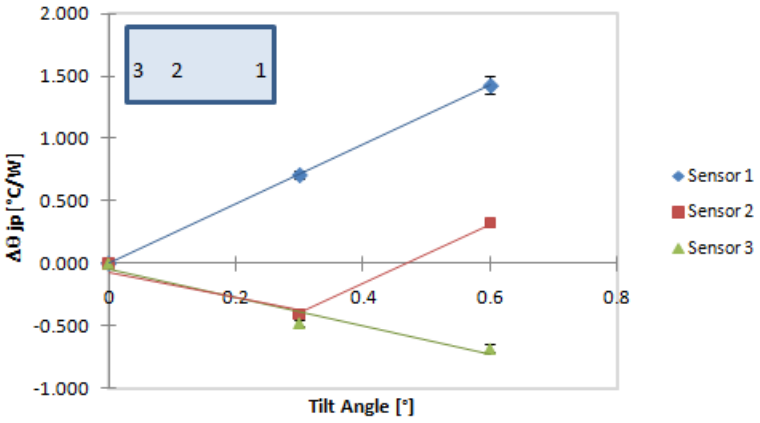

Figure 50. Dry Contact (no TIM) results.

The results for dry contact depicted in Figure 50 show a high impact on the thermal performance of the bare die with respect to tilt angle. Sensor 1 data, a "lift off" edge shows a high increase in delta thermal resistance with the increase in tilt angle. This is expected since

as the tilt angle increases, i.e. as the cooling solution is lifted off this edge the air gap between the cooling solution and the bare die increases. As mentioned in the Introduction, air has a very low thermal conductivity and acts as an insulator, hence yielding a large increase in thermal resistance at this edge.

Sensor 2 can be considered as a pivot point for the discussed experiments. As the tilt angle changes from 0° to 0.3°, more load is applied to the area around sensor 2. This causes a reduction in the air gap at 0.3° angle and hence a reduction in thermal resistance at this point. However, as the tilt angle further changes from 0.3° to 0.6° the cooling solution lifts off of the sensor area creating a larger air gap and therefore causing the thermal resistance to increase.

Sensor 3 is located at the "press" down edge of the die. More pressure is applied to the edge as the tilt angle increases. An increase in pressure at the edge reduces the air gap and hence improvement in thermal resistance with increase in tilt angle is observed.

All the changes in $\Delta\theta_{jp}$ for dry contact are quite large. For example the delta thermal resistance for Sensor 1 between 0° and 0.6° was found to be ~ 1.4°C/W. With such impact of tilt angle to dry contact thermal performance of bare die, it is important to further examine it for the selected TIMs.

4.2.2 Thermal Grease

The same experimental procedure as for dry contacts was applied to the thermal grease. Tilt angle impact on die thermal performance with applied thermal grease is summarize in Figure 51. Once again at Sensor 1 edge of the die, the thermal performance decreases, i.e. thermal resistance increases, with the increase in tilt angle. However, the impact of the tilt angle is not as severe as that of the dry contact. For thermal grease, the thermal resistance change between 0° and 0.6° tilt is approximately 0.07°C/W which is significantly lower than of the dry contact.

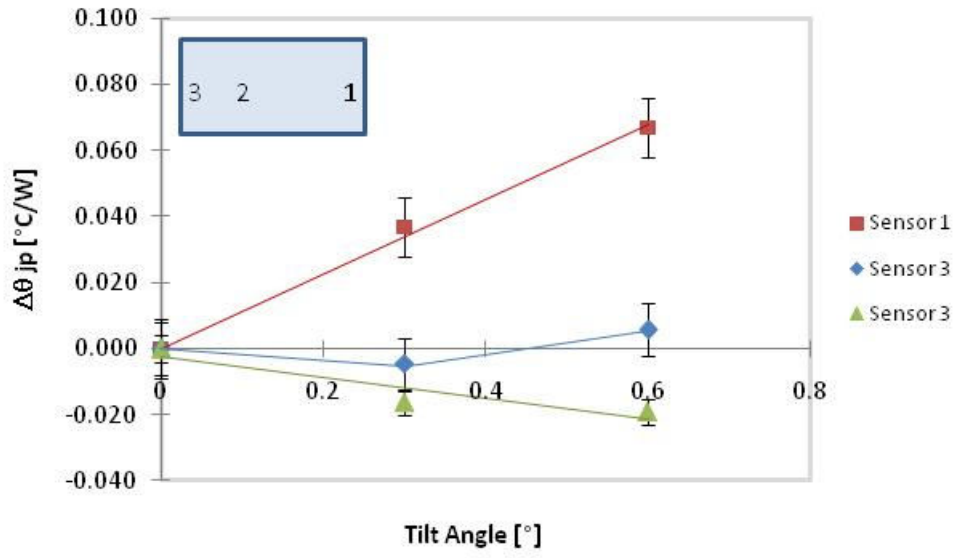

Figure 51. Thermal grease results.

For the thermal grease TIM, Sensor 2 still acts as a “pivot” point so there is a reduction in thermal resistance between 0° and 0.3° tilt followed by an increase between 0.3° and 0.6° tilt. However, one should notice

that the change in both angles is really low--on the order of 0.005°C/W--which is within the accuracy of the measurement and can therefore be considered as no significant change in performance at this point.

Finally, results at the press down edge, Sensor 3, for thermal grease show some improvement in performance on the order of ~ 0.016°C/W at 0.3° tilt and ~ 0.019°C/W at 0.6° tilt. Therefore, no significant change between 0.3° and 0.6° tilt is observed. This suggests that the minimum BLT at this edge is reached at 0.3° tilt and therefore no further improvements are observed with the increase in pressure as the tilt angle increases.

For comparison purposes of impact of the tilt angle between the dry contact and thermal grease contact, the data are re-plotted for all three sensors in Figures 52 thorough 54.

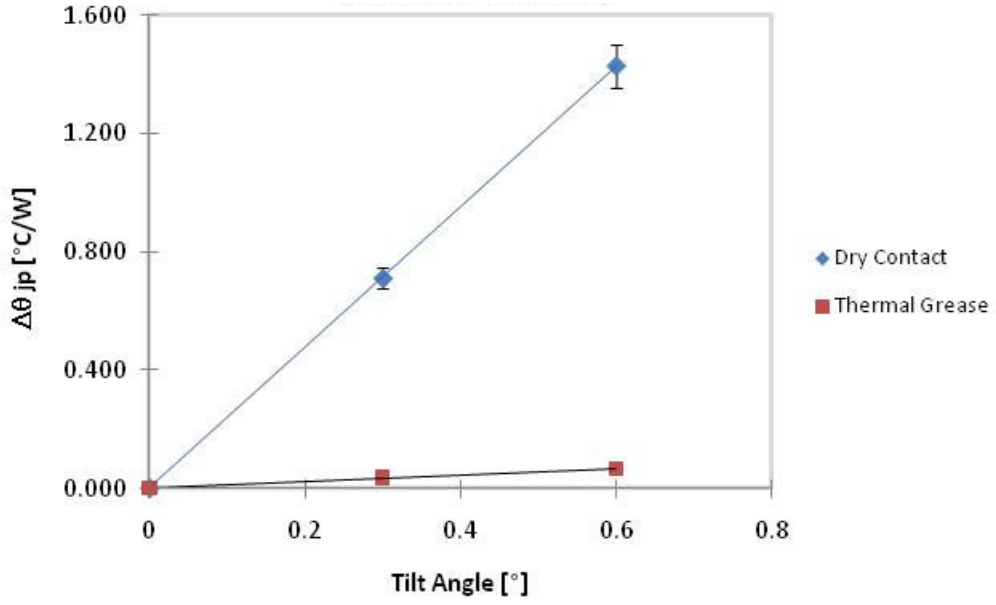

Figure 52. Impact of tilt, thermal grease vs. dry contact sensor 1 results.

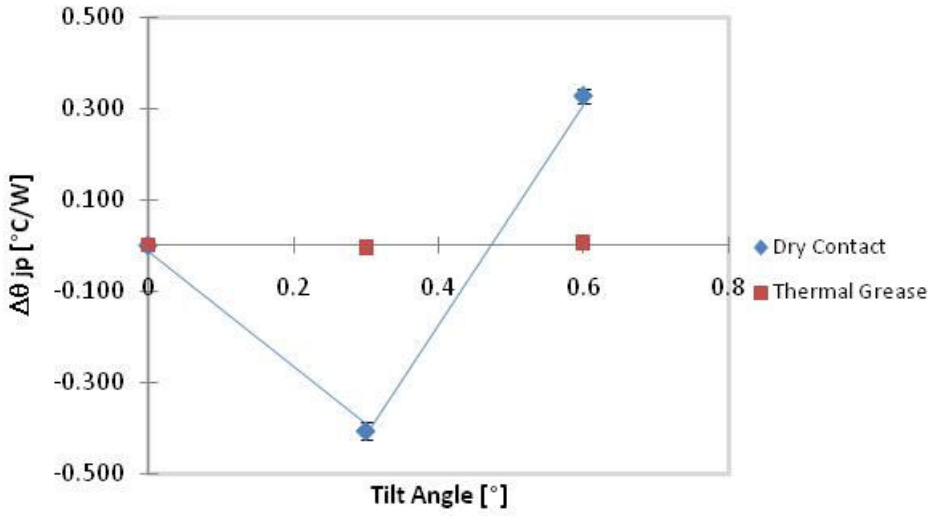

Figure 53. Impact of tilt, thermal grease vs. dry contact sensor 2 results.

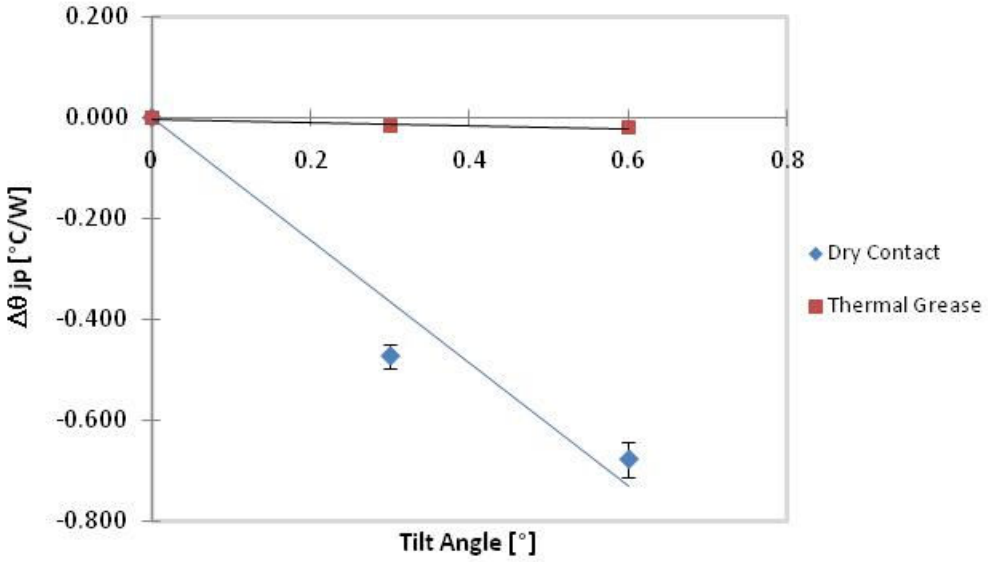

Figure 54. Impact of tilt, thermal grease vs. dry contact sensor 3 results.

4.2.3 Phase Change TIM

Next, a PCM TIM was measured under the same experimental procedure. The results are summarized in Figures 55, 56 and 57 for Sensors 1, 2 and 3 respectfully. Tilt angle has a very similar impact on bare die thermal performance when PCM is used compared to grease. Once again, at the Sensor 1 edge, a negative impact on thermal resistance is observed with the increase in tilt angle as evident from Figure 55. No significant impact is observed at the Sensor 2 and Sensor 3 locations.

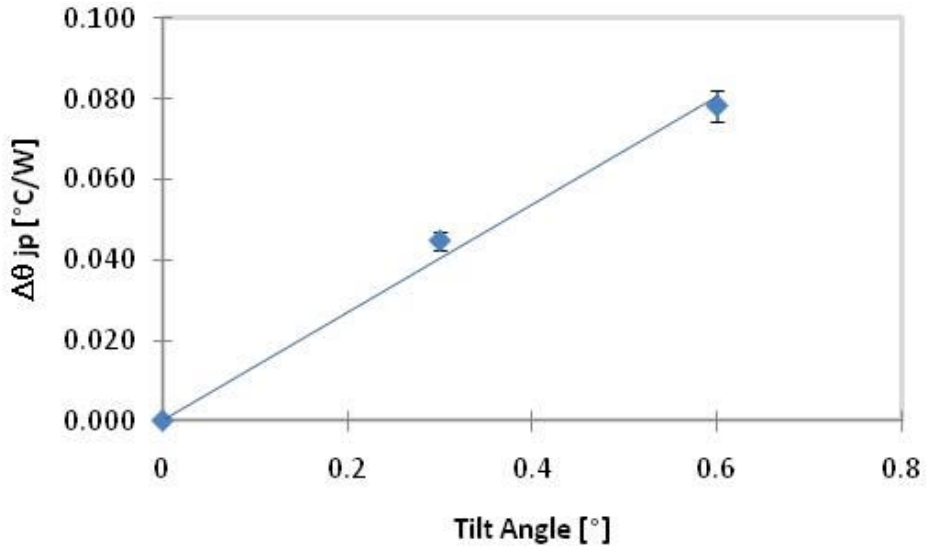

Figure 55. PCM results for sensor 1.

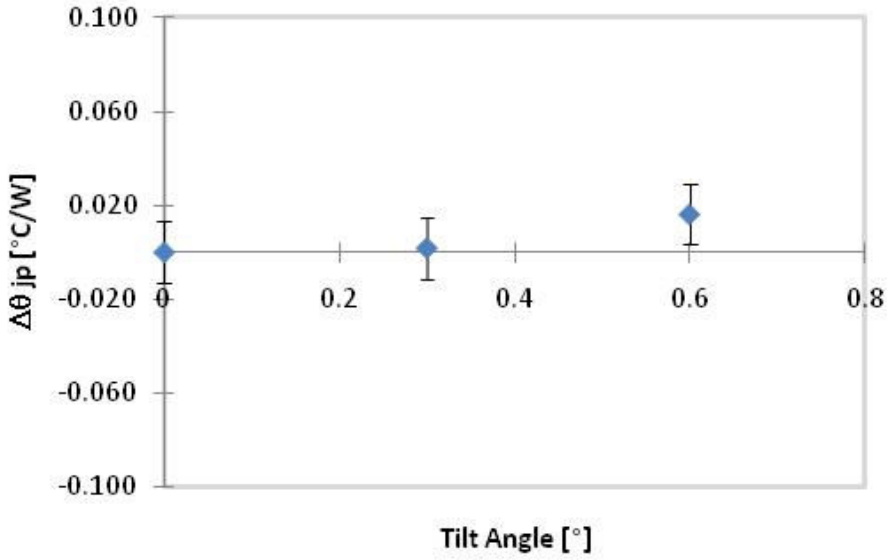

Figure 56. PCM results for sensor 2.

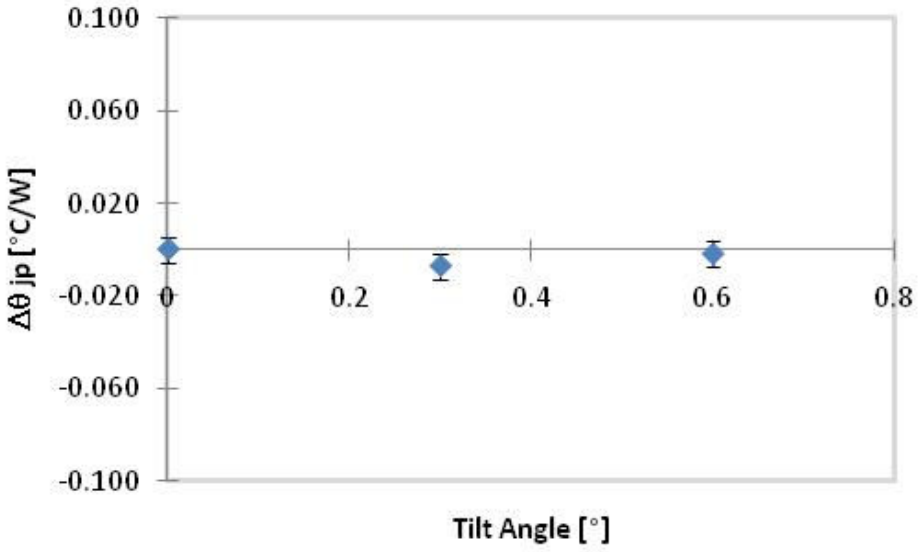

Figure 57. PCM results for sensor 3.

Once again, for comparison purposes, thermal grease data along with PCM data for all three sensors are re-plotted and are shown in Figures 58 through 60. As mentioned, there is no significant difference in the performance trends between these two materials.

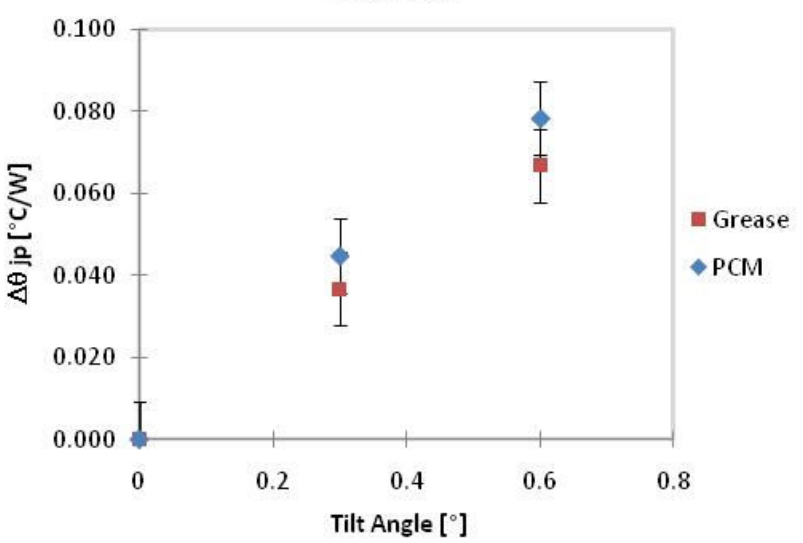

Figure 58. Impact of tilt, thermal grease vs. PCM sensor 1 results.

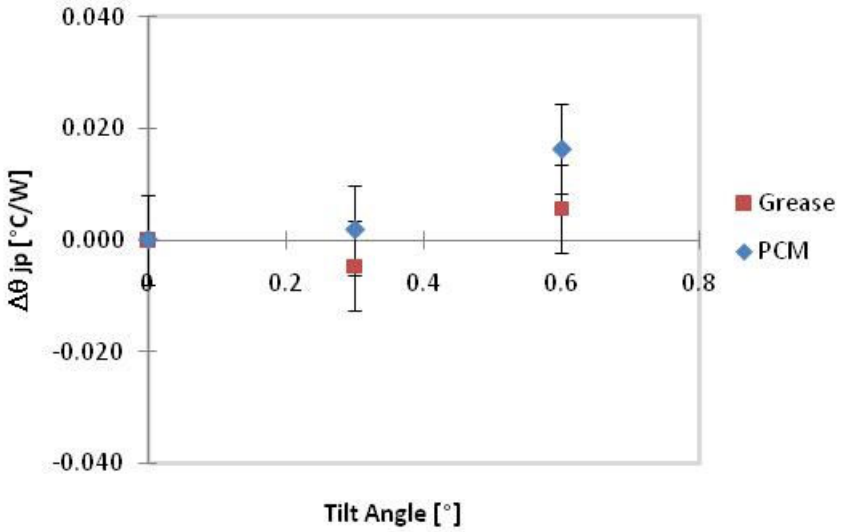

Figure 59. Impact of tilt, thermal grease vs. PCM sensor 2 results.

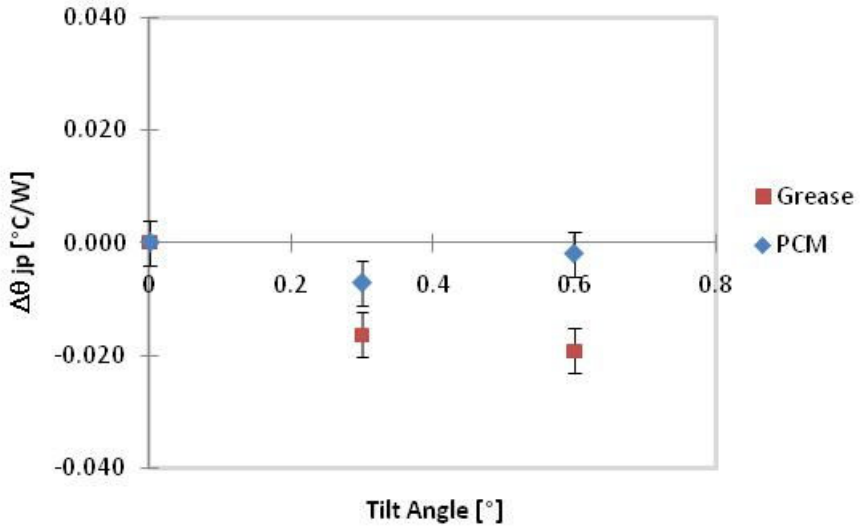

Figure 60. Impact of tilt, thermal grease vs. PCM sensor 3 results.

4.2.4 Gap Fillers

Finally data were collected using the same procedure for two gap fillers. The results for type 1 gap filler for all three preform thicknesses and Sensors 1, 2 and 3 are presented in Figures 61 through 63.

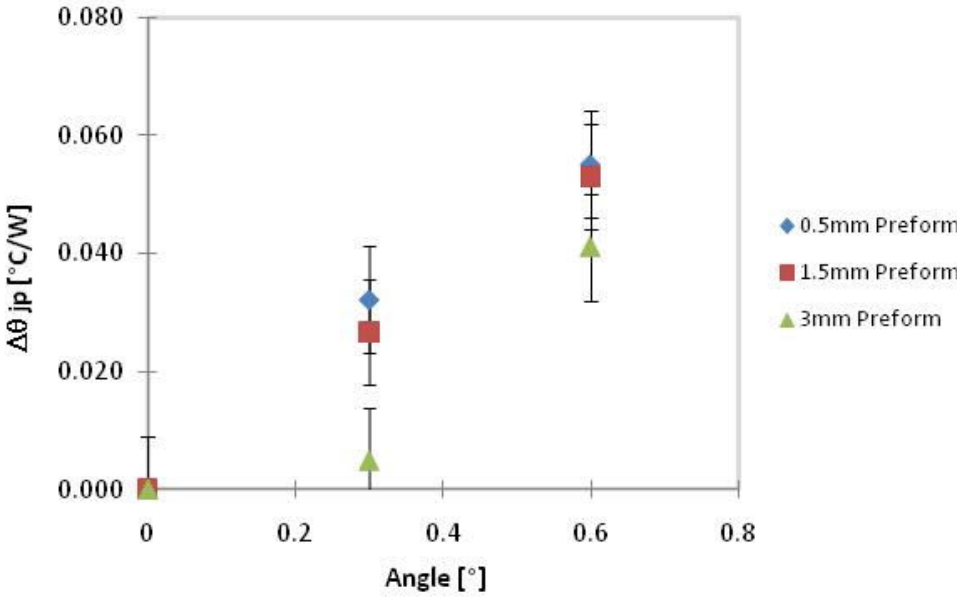

Figure 61. Gap filler type 1, results for sensor 1.

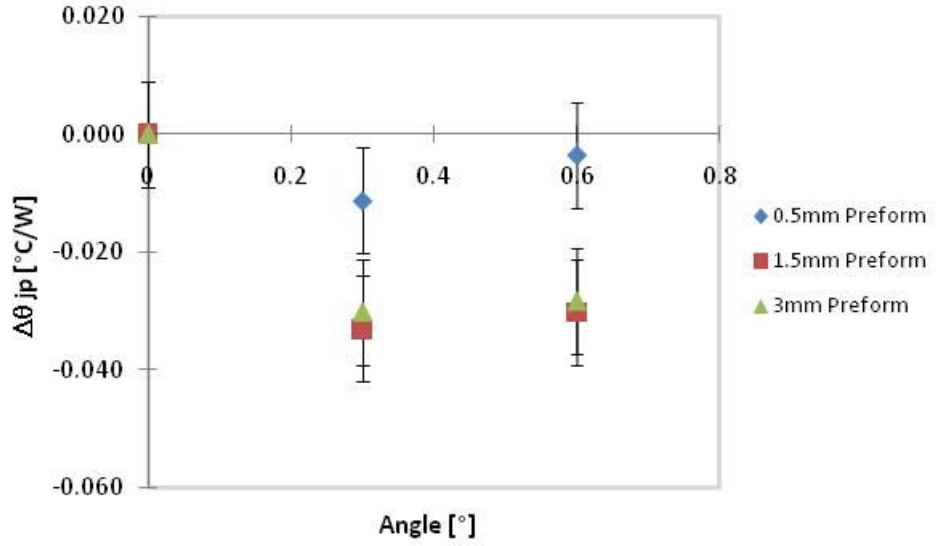

Figure 62. Gap filler type 1, results for sensor 2.

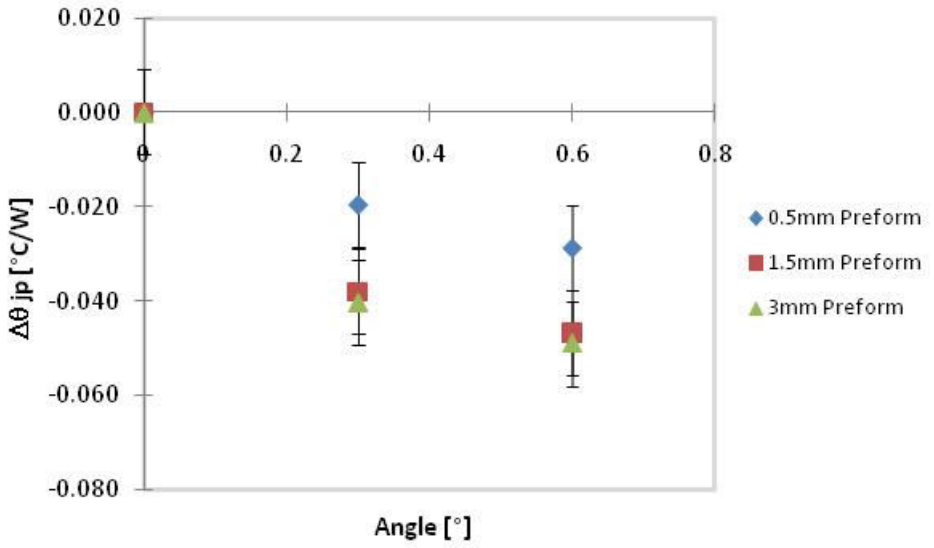

Figure 63. Gap filler type 1, results for sensor 3.

Compared to dry contact, the impact of tilt angle on thermal performance was not as severe when gap filler type 1 was used. However, as was found from the results of the Angular TIM Tester, pressure along with preform thickness of the gap filler play a significant role on the thermal performance of this type of material. For this reason, the higher pressure experienced in the region of Sensor 2 and Sensor 3 with the increase of tilt angle shows higher improvement for thicker material samples. Therefore, the reduction of the BLT of the gap filler material significantly impacts its performance. The same conclusions can be made for the gap filler type 2 material whose results are presented in Figures 64 through 66.

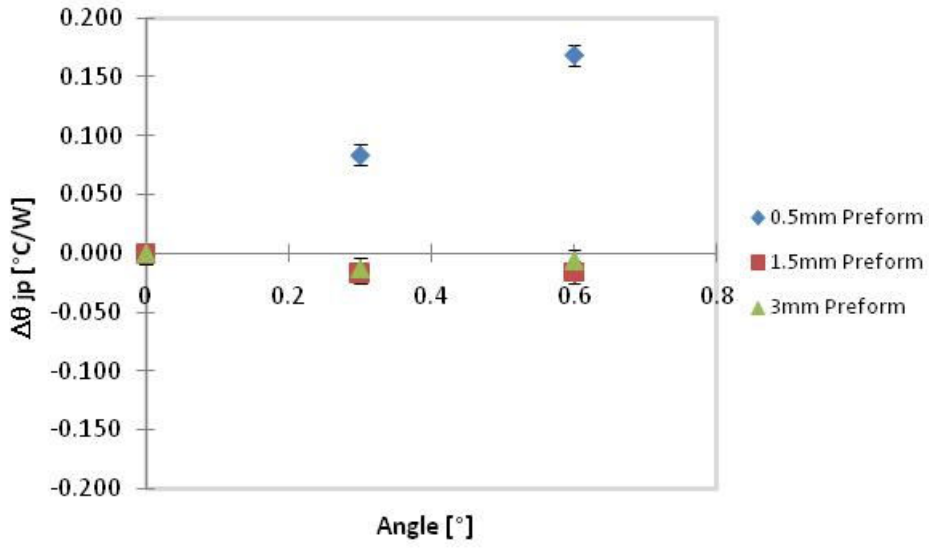

Figure 64. Gap filler type 2, results for sensor 1.

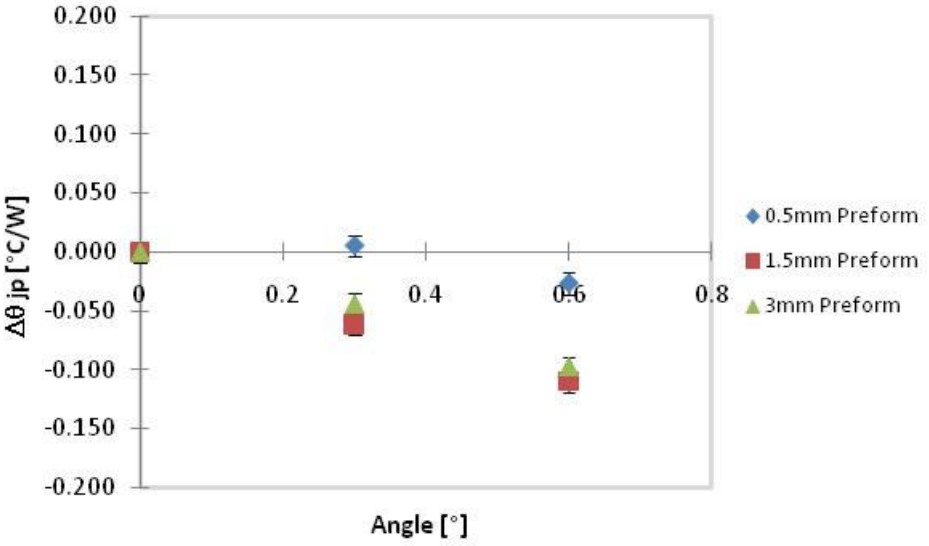

Figure 65. Gap filler type 2, results for sensor 2.

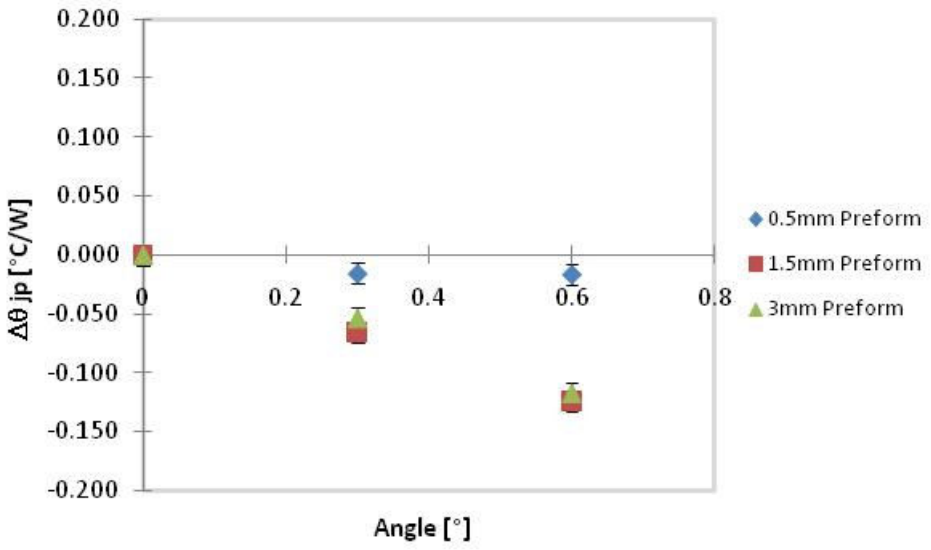

Figure 66. Gap filler type 2, results for sensor 3.

4.3 Angular TIM Tester vs. Bare Die Tilting Metrology

For comparison, the change in thermal resistance vs. tilt angle data obtained from both metrologies for thermal grease and PCM are plotted in Figures 67 and 68. The Bare Die Tilting Metrology results are plotted for sensor 1 and results obtained on the Angular TIM tester for all pressures. Results for these two types of material are in close agreement between the two metrologies as illustrated in Figures 67 and 68.

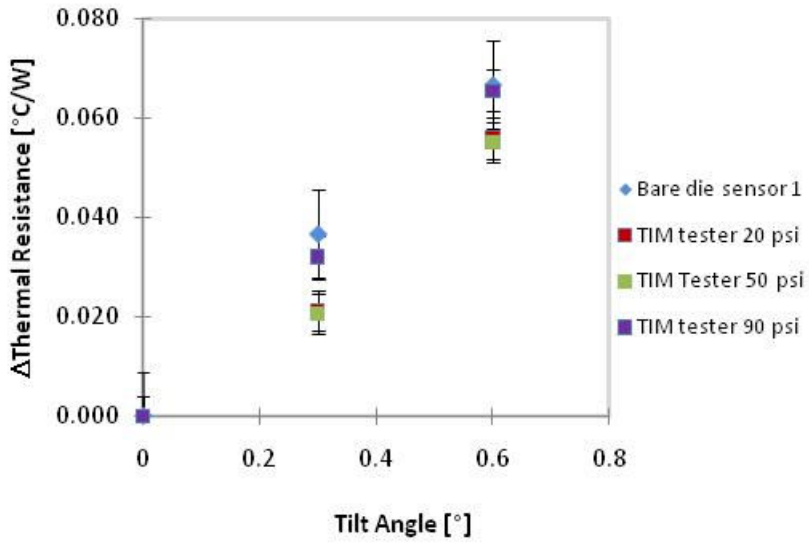

Figure 67. Change in thermal resistance vs. tilt angle - Angular TIM Tester and Bare Die Tilting metrology results for thermal grease.

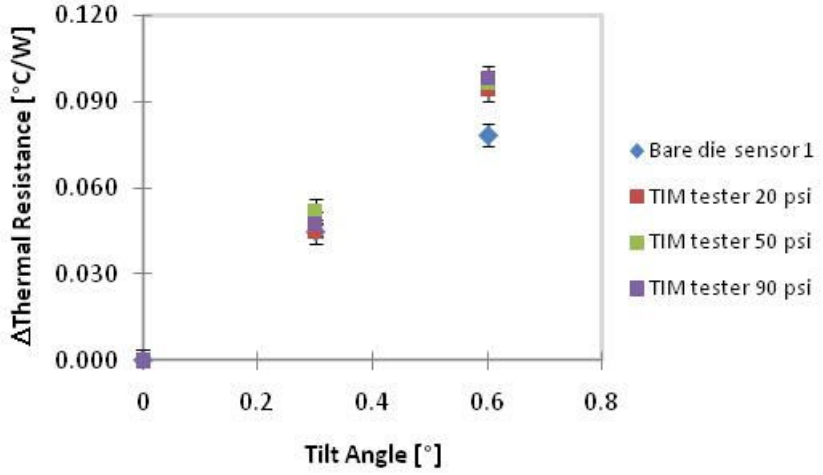

Figure 68. Change in thermal resistance vs. tilt angle - Angular TIM Tester and Bare Die Tilting metrology results for PCM.

Chapter 5

SUMMARY AND CONCLUSION

Two different metrologies were developed to characterize TIMs under induced tilt. The first metrology, “Angular TIM Tester”, is based on 1D steady state heat conduction where a TIM sample is placed between two copper rods and the temperature is recorded along the rods’ lengths using thermocouples. The advantage of the developed metrology is that the rods can be subjected to a specified tilt angle. In addition, the thickness of the TIM under test is measured by a capacitance gauge located very close to the sample hence compensating for the thermal expansion of the rods during test.

The second metrology, “Bare Die Tilting Metrology”, was developed for in-situ TIM characterization. The metrology measures thermal resistance between the junction of the bare die package and thermal solution. As with the first metrology, the advantage of the second metrology is that an angle of tilt can be induced between the package and the cooling solution.

To qualify the developed metrologies, five different commercially available TIMs were selected for measurement. Two types of thermal grease were selected based on the fact that thermal greases are the most commonly used TIMs in the electronic package industry. Next, a phase change material was selected based on its good thermal performance, wide usage and ability to conform at temperatures above its phase change

temperature. Finally, two types of gap fillers were also studied. The gap fillers were selected as they are widely used to fill large gaps between two mating surfaces.

Experimental results obtained from the Angular TIM tester showed an impact of tilt angle on the thermal performance of grease type and phase change materials. Data were collected at relatively small tilt angles, 0.3° and 0.6°, for all materials. The results for thermal grease and PCM showed an increase in thermal resistance with an increase in tilt angle. For grease (type 1), the thermal impedance increased by ~60% and for PCM by ~130% between 0° and 0.6° tilt at low pressure (20 psi). On the other hand, the results for gap filler materials tested in the Angular TIM tester showed no significant impact on their thermal resistance with the increase in tilt angle.

Numerous studies, along with this one, have shown that the thermal resistance of a TIM usually increases with increasing bond line thickness (BLT) [33]. The change in tilt angle causes a change in BLT of the TIM. As the surfaces are tilted the resulting BLT is not uniform across the cross-sectional area.

In addition to non-uniform BLT under tilted conditions, the pressure is also not uniform under these conditions. The pressure plays a key role in thermal interface material performance [34]. This was also evident from the experimental results in the current study. It was shown that for all types of materials tested in the Angular TIM tester, the thermal resistance

of the selected TIM decreased with an increase in pressure. For thermal grease (type 1) and PCM, the thermal impedance reduced by ~20% by increasing pressure from 20 to 50 psi at 0° angle. For gap fillers the impedance reduced on average by ~30% by an increase in pressure from 20 to 50 psi at 0° angle across all thicknesses. An increase in pressure reduces the BLT of the TIM and also improves the contact resistance between the TIM and the mating surfaces (in this case copper rods), thereby improving the overall resistance of the TIM.

In-situ testing performed in the Bare Die Tilting metrology showed significant impact on bare die thermal performance for dry contact, i.e. no TIM with increasing tilt angle. For dry contact the change in thermal resistance for Sensor 1 (lift off edge) between 0° and 0.6° angles was found to be ~ 1.4°C/W. Dry contact data only confirmed the need for TIMs in electronic package applications. The results for grease and phase change material showed lower impact on junction-to-plate thermal resistance for bare die package, but nevertheless did show impact. For the grease the change in thermal resistance for Sensor 1 (lift off edge) between 0° and 0.6° angles was found to be ~0.07 and for PCM ~0.08°C/W.

The results for gap filler materials were somewhat different. In the Angular TIM Tester, no significant impact on TIM resistance for these materials was observed with an increase in tilt angle. However, this was not the case for in-situ testing further proving that TIM material

characterization should be performed in the actual applications for their performance to be verified. For example, for 0.5-mm-thick preform gap filler the change in thermal resistance between 0° and 0.6° angles was found to be ~0.16°C/W for Sensor 1. Even though the tilt angle showed impact on gap filler performance for in-situ tests, pressure and material thickness played a greater role in their performance. So, for thicker gap filler materials, no significant change was observed at the Sensor 1 location with an increase in tilt angle. However, at the Sensor 3 location where more pressure is applied once tilt is induced, an improvement in thermal resistance of ~0.12°C/W is observed. This indicates that for thicker gap fillers, pressure plays an important role in the performance of the TIM.

In summary, analyzing TIM materials under different tilt angles helps thermal design engineers select appropriate materials for specific applications. In addition, given the performance of TIMs under induced angle of tilt can help assembly process and design engineers set specifications for allowed angle of tilt for each or all components within a given assembly. Though, for the best thermal performance, no tilt should be allowed, this is not a realistic scenario. In addition, relaxing the specifications when and if possible can reduce the overall cost of the component and/or assembly process.

REFERENCES

[1] G. E. Moore, "Cramming More Components Onto Integrated Circuits," *Proceedings of the IEEE,* vol. 86, pp. 82-85, 1998.

[2] M. Mahalingam, "Thermal management in semiconductor device packaging," *Proceedings of the IEEE,* vol. 73, pp. 1396-1404, 1985.

[3] J. Xu and T. S. Fisher, "Enhancement of thermal interface materials with carbon nanotube arrays," *International Journal of Heat and Mass Transfer,* vol. 49, pp. 1658-1666, 2006.

[4] T. Tao*, et al.*, "Dense Vertically Aligned Multiwalled Carbon Nanotube Arrays as Thermal Interface Materials," *Components and Packaging Technologies, IEEE Transactions on,* vol. 30, pp. 92-100, 2007.

[5] W. WenXuan*, et al.*, "New Nano-Thermal Interface Materials (Nano-TIMs) with SiC Nano-Particles Used for Heat Removal in Electronics Packaging Applications," in *Electronic Materials and Packaging, 2006. EMAP 2006. International Conference on*, 2006, pp. 1-5.

[6] A. Yu*, et al.*, "Graphite Nanoplatelet−Epoxy Composite Thermal Interface Materials," *The Journal of Physical Chemistry C,* vol. 111, pp. 7565-7569, 2007/05/01 2007.

[7] C. K. D. P. Jaiswal, "Thermal Interface Materials used for Improving the Efficiency and Power Handling Capability of Electronic Devices: A Review," *INTERNATIONAL JOURNAL OF INNOVATIVE TECHNOLOGY & CREATIVE ENGINEERING,* vol. 1, pp. 1-9, May 2011.

[8] T. Ollila, "Navigating the maze of thermal interface materials," *Electronic Products Magazine,* 1999.

[9] Y. JOON LEE, "Thermally Conductive Adhesive Tapes: A Critical Evaluation and Comparison," *Advanced Packaging,* 2007.

[10] B. Rauch, "Understanding the performance characteristics of phase-change thermal interface materials," in *Thermal and Thermomechanical Phenomena in Electronic Systems, 2000. ITHERM 2000. The Seventh Intersociety Conference on*, 2000, p. 47.

[11] K. Young, "Thermal Gap Fillers: New Material Overcomes Performance Trade-Offs," *Thermal Management, Available: http://www.chomerics.com/products/documents/Gap_Filler_Article_2.pdf,* 2007.

[12] Y. Xu*, et al.*, "Sodium Silicate Based Thermal Interface Material for High Thermal Contact Conductance," *Journal of Electronic Packaging,* vol. 122, pp. 128-131, 2000.

[13] A. L. Peterson, "Silicones with improved thermal conductivity for thermal management in electronic packaging," in *Electronic Components and Technology Conference, 1990. ., 40th*, 1990, pp. 613-619 vol.1.

[14] X. Luo*, et al.*, "Thermal Stability of Thermal Interface Pastes, Evaluated by Thermal Contact Conductance Measurement," *Journal of Electronic Packaging,* vol. 123, pp. 309-311, 2001.

[15] T. Sasaski*, et al.*, "Development of sheet type thermal conductive compound using AlN," in *Electronic Manufacturing Technology Symposium, 1995, Proceedings of 1995 Japan International, 18th IEEE/CPMT International*, 1995, pp. 236-239.

[16] C. Chia-Pin*, et al.*, "An accelerated reliability test method to predict thermal grease pump-out in flip-chip applications," in *Electronic Components and Technology Conference, 2001. Proceedings., 51st*, 2001, pp. 91-97.

[17] C. Chia-Pin*, et al.*, "Application of phase-change materials in Pentium (R) III and Pentium (R) III Xeon^{TM} processor cartridges," in *Advanced Packaging Materials: Processes, Properties andInterfaces, 2000. Proceedings. International Symposium on*, 2000, pp. 265-270.

[18] J. Virendra*, et al.*, "Flip chip assembly challenges using high density, thin core carriers," in *Electronic Components and Technology Conference, 2005. Proceedings. 55th*, 2005, pp. 314-319 Vol. 1.

[19] C. C.-P. Prasher R., Mahajan R., , "Thermal interface materials: a brief review of design characteristics and materials," *Electronics Cooling,* February 2004.

[20] R. Mahajan, Nair, R., Wakharkar, V., Swan, J., Tang, J., and Vandentop, G., , "Emerging Directions for Packaging

Technologies," *Intel Technology Journal, Semiconductor Technology and Manufacturing,* vol. 6, 2nd Quarter, 2002 2002.

[21] R. Mahajan, Brown, K., and Atluri, V, "The Evolution of Microprocessor Packaging," *Intel Journal of Technology,* 3rd Quarter, 2000 2000.

[22] R. Mahajan*, et al.*, "Cooling a Microprocessor Chip," *Proceedings of the IEEE,* vol. 94, pp. 1476-1486, 2006.

[23] S. G. L. Chu C.P., Chung Y.D., , "Thermal modeling of grease type interface material in PPGA application," *Proc. 13th IEEE Semi-Therm,* vol. 1, pp. 57-63, 1997.

[24] R. E. Simons, "Thermal Management of Electronic Packages," *Solid State Technology,* pp. 131-136, 1983 1983.

[25] W. R. L. Gwinn J.P., "Performance and testing of thermal interface materials," *Microelectronics Journal* vol. 34, pp. 215-222, 2003.

[26] G. L. Solbrekken*, et al.*, "The development of a tool to predict package level thermal interface material performance," in *Thermal and Thermomechanical Phenomena in Electronic Systems, 2000. ITHERM 2000. The Seventh Intersociety Conference on*, 2000, p. 54.

[27] J. Galloway and S. Kanuparthi, "BLT control and its impact on FCBGA thermal performance," in *Thermal and Thermomechanical Phenomena in Electronic Systems, 2008. ITHERM 2008. 11th Intersociety Conference on*, 2008, pp. 388-394.

[28] R. Schacht*, et al.*, "Characterization of Thermal Interface Materials," in *Electronics Systemintegration Technology Conference, 2006. 1st*, 2006, pp. 1367-1373.

[29] M. Grujicic*, et al.*, "The effect of thermal contact resistance on heat management in the electronic packaging," *Applied Surface Science,* vol. 246, pp. 290-302, 2005.

[30] J. J. W. Tzeng*, et al.*, "Technical review on thermal conductivity measurement techniques for thin thermal interfaces," in *Semiconductor Thermal Measurement and Management Symposium, 2000. Sixteenth Annual IEEE*, 2000, pp. 174-181.

[31] K. Hanson, "ASTM D 5470 TIM material testing," in *Semiconductor Thermal Measurement and Management Symposium, 2006 IEEE Twenty-Second Annual IEEE*, 2006, pp. 50-53.

[32] V. Khuu*, et al.*, "Considerations in the Use of the Laser Flash Method for Thermal Measurements of Thermal Interface Materials," *Components, Packaging and Manufacturing Technology, IEEE Transactions on,* vol. 1, pp. 1015-1028, 2011.

[33] C. Chia-Pin*, et al.*, "Thermal modeling and experimental validation of thermal interface performance between non-flat surfaces," in *Thermal and Thermomechanical Phenomena in Electronic Systems, 2000. ITHERM 2000. The Seventh Intersociety Conference on*, 2000, p. 62.

[34] L. Bharatham*, et al.*, "A Study of Application Pressure on Thermal Interface Material Performance and Reliability on FCBGA Package," in *Electronic Materials and Packaging, 2006. EMAP 2006. International Conference on*, 2006, pp. 1-7.